

This item was submitted to Loughborough's Institutional Repository (<https://dspace.lboro.ac.uk/>) by the author and is made available under the following Creative Commons Licence conditions.



CC creative commons
COMMONS DEED

Attribution-NonCommercial-NoDerivs 2.5

You are free:

- to copy, distribute, display, and perform the work

Under the following conditions:

 **Attribution.** You must attribute the work in the manner specified by the author or licensor.

 **Noncommercial.** You may not use this work for commercial purposes.

 **No Derivative Works.** You may not alter, transform, or build upon this work.

- For any reuse or distribution, you must make clear to others the license terms of this work.
- Any of these conditions can be waived if you get permission from the copyright holder.

Your fair use and other rights are in no way affected by the above.

This is a human-readable summary of the [Legal Code \(the full license\)](#).

[Disclaimer](#) 

For the full text of this licence, please go to:
<http://creativecommons.org/licenses/by-nc-nd/2.5/>

**Dynamic Effects in Capillary Pressure-Saturations Relationships for
Two-Phase Flow in 3D Porous Media: Implications of
Micro-Heterogeneities**

Mahsanam Mirzaei, Diganta Bhusan Das¹

Department of Engineering Science, Oxford University, Oxford OX1 3PJ, UK

Revised Version Submitted for Publication in the Journal:

Chemical Engineering Science

24 November 2006

¹Author for correspondence (Email: Diganta.Das@eng.ox.ac.uk; Tel: 0044 1865 283454)

Dynamic Effects in Capillary Pressure-Saturations Relationships for Two-Phase Flow in 3D Porous Media: Implications of Micro-Heterogeneities

Mahsanam Mirzaei, Diganta Bhusan Das*

Department of Engineering Science, the University of Oxford, Oxford OX1 3PJ, UK

ABSTRACT

The capillary pressure-saturation (P^c -S) relationships are essential in characterizing two-phase flow behaviour in porous media. However, these relationships are not unique and depend on the flow dynamics, i.e., steady state or dynamic, among other factors. It has been shown that empirical models describing two-phase flow processes in porous media may be inadequate to account fully for the physics of flow in dynamic conditions. New capillary pressure relationships have been proposed which include an additional term to account for the dependence of capillary pressure on saturation and time derivative of saturation ($\partial S/\partial t$). This parameter is a capillary damping coefficient, also known as dynamic coefficient (τ), which establishes the speed at which flow equilibrium is reached. The dependence of P^c -S relationships on $\partial S/\partial t$ is called *dynamic effects*.

In most laboratory experiments for measuring two-phase flow properties, it is implicitly assumed that the sample is homogeneous. However, this is not the case and micro-heterogeneities with their distinct multiphase flow properties may exist within the domain. They affect the dynamics of the multiple fluid phases and saturation distributions in the domain. These issues have been studied individually but the combination of dynamic effects and micro-scale heterogeneities on the P^c -S relationships has not been quantified accurately, particularly in 3D domains. Consequently, there are significant uncertainties on the reported values of τ in the literature.

In this work, we have carried out a numerical study to investigate how the presence of micro-scale heterogeneities affects the dynamics of dense non-aqueous phase liquid (DNAPL) and water flow in porous domain. The relative significance of the variations in nature, intensity and distribution of micro-scale heterogeneities on dynamic flow conditions are manifested on P^c -S curves which are quantified in terms of the dynamic coefficient, τ . There is a complex interplay of various factors (e.g., dynamic flow conditions, distribution and intensity of micro-heterogeneity, pore size distribution, domain size and geometry and media anisotropy) which affects P^c -S curves. However, our results show that as the intensity of heterogeneity increases the dynamic coefficient at a given saturation increases, provided all other factors remain the same. The effects of domain shapes (cylindrical v/s rectangle), aspect ratios, dimensionality (2D v/s 3D), permeability anisotropy on τ are also analyzed in order to generalize their effects as far as possible. We envisage that our simulations will minimize some of the inconsistencies on the reported data on τ in the literature.

KEYWORDS: Two-phase flow; Dynamic effects; Dynamic coefficient; Micro-heterogeneity; Porous media; Capillary pressure; Saturation; Relative permeability; Anisotropy; Aspect Ratio

* Author for Correspondence (Email: Diganta.Das@eng.ox.ac.uk; Tel: 0044 1865 283454)

39 1. Introduction

40 A correct description of two-phase flow behaviour in porous media requires the determination of various fluids
41 and media parameters and, the constitutive relationships among capillary pressure (P^c), fluid saturation (S) and
42 relative permeability (K_r). Traditionally, the P^c - S - K_r relationships have been determined under equilibrium
43 conditions. However, these relationships are not unique and their determination for real soil samples is
44 particularly difficult because of two effects: (i) presence of micro-heterogeneities in the flow domain and (ii)
45 dynamic effects in the P^c - S - K_r relationships. Dependence of the P^c - S - K_r relationships on the time derivative of
46 saturation ($\partial S / \partial t$) is known as the dynamic effect (Hassanizadeh et. al., 2002). While the significances of micro-
47 scale heterogeneity and dynamic effect on P^c - S - K_r relationships have been studied individually at different
48 scales of observation, the combination of the two effects are not well characterised, particularly in three-
49 dimensional (3D) porous domains (realistic domains).

50

51 1.1 Steady State Capillary Pressure Relationship

52 Capillary pressure is an essential characteristic of two-phase flow in porous media. In the empirical
53 macroscopic description, P^c is defined as the difference in average non-wetting and wetting phase pressures
54 and is expressed as a function of wetting phase saturation (S) (Collins, 1961; Scheidegger, 1974, Bear and
55 Verruijt, 1987; Helmig, 1997),

$$56 \quad P_{nw} - P_w = P^{c, equ}(S) = f(S) \quad (1)$$

57 where P_{nw} and P_w are the average pressures of the non-wetting and wetting phases, respectively. This
58 relationship is determined under equilibrium conditions, i.e., when $\partial S / \partial t$ is zero in theory or negligible in
59 practice. Equation (1) is implicitly assumed to account for all effects that influence the equilibrium distribution
60 of fluid(s) in porous media, e.g., fluid properties (e.g., surface tension, viscosity ratio), medium properties
61 (e.g., particle and pore size distributions), wettability of solid surfaces to fluid phases, contact angles, media
62 heterogeneities along with any other parameters. In other words, all effects are lumped into the P^c - S
63 relationship (equation 1), which is then said to characterise the two-phase flow behaviour along with the K_r - S
64 relationship. The momentum conservation of the two-phase flow system is generally expressed by an extension
65 of the Darcy's law as shown in equation (5) (Muskat and Meres, 1936; Leverett 1939; Bear, 1972; Helmig,
66 1997). In this extension, it is assumed that each fluid phase maintains its own pathways and hence, the effects
67 of any momentum transfer across the fluid/fluid interfaces (e.g., due to molecular interactions) may be ignored
68 in practice (Whitaker, 1986).

69

70 1.2 Dynamic Capillary Pressure Relationship

71 However, fluids do not necessarily flow under steady conditions, particularly at smaller time periods when the
72 term $\partial S / \partial t$ may be high. This is supported by a number of experimental and theoretical studies that show that
73 the capillary pressure relationships depend on the flow conditions, i.e. whether it is at steady or unsteady state
74 (Topp et. al., 1967; Vachaud, 1972; Kalaydijan, 1992; Wildenschild, 2001; Barenblatt et. al., 2003; Singh and
75 Mohanty, 2003; Tsakiroglou et. al., 2003; Oung et. al., 2005; Wildenschild et. al., 2005; Das et. al., 2006;
76 Berentsen et. al., 2006; Bottero et. al., 2006; Mirzaei et. al., 2006; Porter et. al., 2006). There are therefore an

77 increasing number of authors who suggest that the conventional steady state capillary pressure relationship
 78 (equation 1), which assumes that P^c is a unique function of fluid saturation, may not be sufficient to
 79 characterize the two-phase flow behaviour under dynamic conditions (Kalaydjian, 1992; Hassanizadeh and
 80 Gray, 1993; Beliaev and Hassanizadeh, 2001; Beliaev and Schotting, 2002; Hassanizadeh et. al., 2002; Dahle
 81 et. al., 2005; Hanyga and Seredynska, 2005; O'Carrol et. al., 2005; Oung et. al., 2005; Nordbotten et. al.,
 82 2006).

83

84 To take into account the dynamic capillary pressure effects on two-phase flow behaviour in porous media,
 85 Hassanizadeh and Gray (1993) have proposed a theory, which indicates that the conventional P^c -S
 86 relationships (equation 1) can be generalized to include a capillary damping or dynamic coefficient τ as below:

$$87 \quad \left(P^{c,dyn} - P^{c,equ} \right)_s = -\tau \left(\partial S / \partial t \right)_s \quad (2)$$

88 where $P^{c,dyn}$ is the dynamic capillary pressure $\left(P_{nw}^{dyn} - P_w^{dyn} \right)$, $P^{c,equ}$ is the capillary pressure at equilibrium
 89 conditions $\left(P_{nw}^{equ} - P_w^{equ} \right)$, and $\partial S / \partial t$ is the time derivative of saturation, all measured at the same fluid saturation
 90 value (S). As evident, equation (2) has the general form of a straight line and, in this form, should pass through
 91 the origin. The slope of this linear relationship is the capillary damping coefficient or the dynamic coefficient
 92 (τ). Among other factors, τ depends on medium and fluid properties, degree of saturation and types of
 93 heterogeneity (fractures, layers, etc), if any. If τ is small, the equivalence between $P^{c,dyn}$ and $P^{c,equ}$ is
 94 established quickly. On the other hand, the necessary time period to reach equilibrium is high for a large value
 95 of τ . Thus, the dynamic coefficient behaves as a capillary damping coefficient and indicates the dynamics of
 96 the two-phase flow system.

97

98 One may argue that the dynamic effects can be studied by the use of Capillary number (Ca), which provides an
 99 indication of dynamic effects caused by flow rate at domain boundaries. However, this dynamic rate effect is
 100 not the issue here. The dynamic effect investigated in this paper is related to the fact that fluid/fluid interfaces
 101 need a finite relaxation time to reach their equilibrium positions at given pressure conditions (Barenblatt et. al.,
 102 1990). If the conventional P^c -S relationship is employed to define the dynamic capillary pressure, it is
 103 implicitly implied that any disturbance in the system is eliminated instantaneously or within a short period of
 104 time. In other words, for the P^c -S-K_r relationships to be independent of dynamic effects, the two-phase system
 105 should not be affected by flow conditions. This is contrary to a number of experimental studies, as discussed
 106 before. Therefore, in the last few years, the significance of dynamic effects has been investigated in the
 107 contexts of various two-phase flow processes in porous media.

108

109 Beliaev and Hassanizadeh (2001) and Beliaev and Schotting (2002) have tested dynamic P^c -S relationships
 110 and τ for hysteretic effects, respectively. Theodoropoulou and co-workers (Tsakiroglou et. al., 2003;
 111 Tsakiroglou, 2005; Theodoropoulou et. al., 2005) have studied dynamic two-phase flow involving various
 112 Newtonian and non-Newtonian fluids. Hassanizadeh et. al. (2002) have reported that the dynamic coefficient
 113 varies in the range $3 \times 10^4 - 5 \times 10^7 \text{ kgm}^{-1} \text{ s}^{-1}$. Gielen et. al. (2005) have adopted a dynamic pore-scale network

114 model to simulate a ‘flow through type cell’, often used in the measurement of P^c - S - K_r relationships. They
115 have constructed three rectangular networks (3D) of different domain size (5×10^{-3} - 10^{-2} m in length) and have
116 shown that the dynamic coefficients increase with the increase in the averaging network size up to a maximum
117 of $1.2 \times 10^5 \text{ kg m}^{-1} \text{ s}^{-1}$ for the largest pore network they have chosen. Dahle et. al. (2005) have presented a
118 simple 2D pore scale modelling approach based on a bundle of capillary tubes model. Their prime aim has
119 been to demonstrate the pore-scale processes that underlie the dynamic capillary pressure effects. Therefore
120 they adopt a small domain size ($\sim 10^{-3}$ m). As expected, Dahle et. al. obtain small values of τ which range
121 between 10^2 - $10^3 \text{ kg m}^{-1} \text{ s}^{-1}$. Manthey et. al. (2005) have performed numerical experiments on a number of 2D
122 rectangular homogeneous and heterogeneous domains with dimensions varying between 0.12 m and 1.0 m.
123 Their simulations correspond to the ‘flow through’ type cells. Manthey et. al. have shown that the magnitude
124 of τ depends on the boundary conditions, the domain size and various hydraulic parameters of porous
125 materials. Manthey et. al. ignore the effects of dimensionality (2D v/s 3D) and gravity on the dynamic
126 coefficient and show that the values of τ may be as large as $10^9 \text{ kg m}^{-1} \text{ s}^{-1}$ for a domain size of $1.0 \text{ m} \times 1.0 \text{ m}$.
127 They also show that for the 2D domains they have chosen, there is negligible difference in the values of τ in
128 homogeneous (with effective properties) and heterogeneous domain. We show later in our paper that τ depends
129 strongly on the intensity of heterogeneity, i.e., the amounts of heterogeneities embedded in a porous material.
130 Das and Hassanizadeh (2005) have discussed a number of the above papers (Dahle et. al., 2005; Gielen et. al.,
131 2005; Manthey et. al., 2005). Some of these studies have also been reviewed by O’Carrol et. al. (2005)
132 recently. Based on an inverse modelling approach coupled with an algorithm for optimisation of capillary
133 pressure relationships, O’Carrol et. al. have determined τ in the range 1×10^6 – $5.7 \times 10^7 \text{ kg m}^{-1} \text{ s}^{-1}$ for a porous
134 material of permeability $\sim 10^{-11} \text{ m}^2$. In another recent study, Oung et. al. (2005) have obtained static and
135 dynamic P^c - S curves using a geo-centrifugal facility at 15g and 30g for a material of permeability $\sim 10^{-12} \text{ m}^2$.
136 Based on the difference between these curves, Oung et. al. have obtained τ in the range 0 – $600 \text{ kg m}^{-1} \text{ s}^{-1}$ at
137 15g and 10 - $52 \text{ kg m}^{-1} \text{ s}^{-1}$ at 30g. Both O’Carrol et. al. (2005) and Oung et. al. (2005) have used 3D cylindrical
138 porous domains (homogeneous), the same fluids system (Perchloroethylene(PCE)-water) and similar material
139 properties. However, the size of the porous samples and, the experimental and boundary conditions are
140 different in their studies. Consequently both groups of authors obtain distinctly different values of τ . Despite
141 these obvious factors affecting τ , we also believe that the material properties at the smallest scale (e.g. pore
142 and particle size distributions), which affect the bulk material properties (e.g. porosity, permeability, etc), may
143 have influenced the dynamics of two-phase flow studied by O’Carrol et. al. (2005) and Oung et. al. (2005).
144 This is discussed again later when we show that the dynamic capillary pressure depend strongly on the pore-
145 size distribution, given by a coefficient in the Brooks-Corey formulation (Brooks and Corey, 1964).

146

147 As evident from the above discussion, there is a significant variation on the reported values of τ in the
148 literatures (0 – $10^9 \text{ kg m}^{-1} \text{ s}^{-1}$) depending on the size (10^{-3} m – 1 m) and geometry (2D or 3D) of domains,
149 boundary conditions, porous medium properties (e.g., permeability, entry pressure), fluid properties, types of
150 experiments (e.g., flow through cells or geocentrifuge), type of heterogeneities (e.g., uniform or random micro-

151 heterogeneities), etc. Therefore, in principle, one cannot compare directly the values obtained in one study
152 with those obtained in another. One also observes that most of these studies so far have calculated τ for
153 simplified cases, e.g., homogeneous domain, 2D domain with zero gravity effects, bundle of capillary tubes,
154 etc. This causes a practical difficulty in gauging realistic values of τ and consequently using them in predicting
155 dynamic capillary pressure relationships in real life problems, which generally involve complex domain
156 characteristics. There is therefore a need to carry out systematic analyses on the sensitivity of the dynamic
157 coefficient to various factors that govern two-phase flow in porous media under realistic conditions (e.g., 3D
158 heterogeneous media), in an attempt to generalise their effects on τ as far as possible.

159

160 We also note that there have been some discussions in the literature on the general form of equation (2) and as
161 to whether the current form shown in equation (2) should include an intercept (C) term that appears in the
162 general equation of a straight line, e.g.,

$$163 \quad P^{c,dyn} - P^{c,equ} = -\tau(\partial S / \partial t) + C \quad (3)$$

164 Results of Hassanizadeh et. al. (2002), Gielen et. al. (2005) and, Manthey et. al. (2005) show that the equation
165 (2) does not necessarily pass through the origin of the coordinate system. Dahle et. al. (2005) have adopted a
166 form similar to equation (3) and attempts to correlate the intercept term (C) with other parameters which define
167 the bundle of capillary tubes model that they have developed. Tsakiroglou et. al. (2003) have used a
168 dimensionless form of equation (2) for their studies without the intercept term. Whatever may be the form of
169 equation used for dynamic capillary pressure, one can envisage that the range of validity/applicability of these
170 correlations (i.e., if they can be fitted to a straight line) become increasingly difficult to ascertain as the domain
171 complexity increases. As far as we know, the validity/applicability of equation (2) has not been discussed for
172 two-phase flow in 3D heterogeneous domain in the literature so far.

173

174 **1.3 Micro-scale Heterogeneity Effects on Static and Dynamic Capillary Pressure Relationships**

175 Many geological formations and soils contain small-scale heterogeneities such as micro-scale lenses of fine
176 sand with distinctly different multiphase flow properties from those of the surrounding media. They occur at
177 length scales below those of typical laboratory devices and, have significant effects on two-phase flow
178 behaviour in porous media and, hence, the resulting P^c -S- K_r relationships (Fulcher et. al., 1985; Delshad et. al.,
179 1987; Schwille, 1988; Kueper and Frind, 1991; Illangasekare et. al., 1995a,b; Avraam and Payatakes, 1995;
180 Blom, 1999; Henderson et. al., 2000; Ataie-Ashtiani et. al., 2001, 2002; Das et. al., 2004, 2006). There are
181 some indications that micro-heterogeneities affect the dynamic coefficient, τ (Hassanizadeh et. al., 2002;
182 Manthey et. al., 2005; Mirzaei et. al., 2006). Most previous studies also show that τ depends on the domain
183 geometry (2D, 3D rectangle or 3D cylindrical). However, it is not certain if the results obtained for 2D
184 heterogeneous domains (e.g., Manthey et. al., 2005) may be used directly for 3D heterogeneous domains
185 (realistic domains) and if geometry of the domain has any effects on τ -S relationships.

186

187 **1.4 Objectives of this Paper**

188 The main objective of this paper is to characterise the implications of micro-heterogeneities on dynamic two-
189 phase flow behaviour in porous materials in terms of the dynamic coefficient (τ). By ‘micro-heterogeneities’
190 we imply fine sand lenses imbedded in coarse background sand. We carry out large numbers of numerical
191 simulations to determine how the interplay of micro-heterogeneities and dynamic flow conditions (given by
192 different pressure boundary conditions) affect the capillary pressure relationships. All simulations are carried
193 out on 3D cylindrical domains, unless otherwise mentioned, for domain dimensions similar to those used in
194 laboratory experiments (12 cm length \times 10 cm diameter).

195

196 To determine the implications of micro-heterogeneities, we define porous media with different intensities (ω)
197 and distributions of heterogeneities. The intensity of heterogeneity (ω) is a non-dimensional parameter given
198 by the ratio of the volume of imbedded fine sand to the total volume of the sample where the background is a
199 coarser sand (Das et. al., 2004, 2006). In this approach, $\omega=0, 1$ define no heterogeneity in the domain, i.e., a
200 homogeneous coarse ($\omega=0$) or fine ($\omega=1$) sand domain. Higher is the value of ω higher is the amount of fine
201 sand in the domain. At $\omega=0.5$, the volume of fine and coarse sand in the domain becomes equal. In cases where
202 $\omega \geq 0.5$, the volume of fine sand is higher than coarse sand and, therefore, the coarse sand gets entrapped in
203 fine sand. In this paper, we attempt to relate the intensity of heterogeneity (ω) to the dynamic coefficient (τ)
204 for cases where fine sand is embedded in coarse sand. Although we vary the amounts of imbedded fine sand in
205 the domain, we make sure that each micro-heterogeneity block is the same in size. In effect, we make sure that
206 the size effect of each micro-heterogeneity on τ is the same and any change on effective static and dynamic
207 capillary pressure relationships on the larger scale is because of the difference in the intensity and distribution
208 of micro-heterogeneities and, not because of the difference in their size.

209

210 Recent works have shown that τ varies non-linearly with fluid saturation (S) (Hassanizadeh et. al., 2002;
211 Manthey et. al., 2005; Bottero et. al., 2006; Mirzaei et. al., 2006). In this paper, we determine the τ - S
212 relationships for 3D heterogeneous domains. Also, based on our results we obtain the τ - S - ω relationships, in
213 an attempt to generalize the effects of micro-heterogeneities on dynamic capillary pressure relationships. We
214 analyse the implications of micro-heterogeneities on steady and dynamic P^c - S curves. The K_r - S curves for
215 various cases are not presented in this paper since they are not used to determine the values of τ . Discussions
216 on K_r - S curves in various cases may be found in the literature (e.g., Hassanizadeh et. al., 2002; Singh and
217 Mohanty, 2003; Das et. al., 2004, 2006; Theodoropoulou et. al., 2005).

218

219 We also determine how the dynamic coefficient is affected by (i) domain geometries (2D rectangle, 3D
220 rectangle and cylinder) (ii) aspect ratio in 3D cylindrical domain (homogeneous and heterogeneous) and, (iii)
221 anisotropic ratios in permeability in 3D cylindrical domains (homogeneous and heterogeneous). In these cases,
222 we maintain the same boundary conditions and material properties, unless otherwise stated. Our main interests
223 in these simulations are to address some of the uncertainties in the significance of τ in the literature, as
224 discussed in sections 1.2 and 1.3.

225

226 Further, we discuss briefly if equation (2) is applicable/valid for cases when micro-heterogeneities are present
 227 in 3D flow domain. This mainly involves analysing whether the equation (2) maintains the general form of a
 228 straight line. With these analyses, we then identify the magnitude of the intercept (C) for 3D heterogeneous
 229 cases, as shown in equation (3). However, note that we do not make any attempt to correlate the intercept with
 230 various parameters that govern the two-phase flow in porous media. This requires a very high number of
 231 simulations and is beyond the scope of this paper.

232

233 2. Descriptions of Numerical Simulations

234

235 2.1 Governing Model Equations

236 The conservation of fluid mass in the two-phase flow system is described by the following equation,

$$237 \frac{\partial}{\partial t} (\phi \rho_\gamma S_\gamma) + \nabla \cdot (\rho_\gamma q_\gamma) = 0 \quad \text{for } \gamma \equiv w, nw \quad (4)$$

238 where, $\phi[-]$ is porosity, $S_\gamma[-]$ is the saturation of corresponding phase, $\rho_\gamma [\text{Kg m}^{-3}]$ is the fluid density and
 239 $q_\gamma [\text{m}^3 \text{s}^{-1}]$ is the fluid flux. In addition, the multiphase version of Darcy's equation (equation 5) is used to
 240 describe the conservation of fluid momentum in the porous medium.

$$241 \bar{q}_\gamma = -\frac{K_{r\gamma} K}{\mu_\gamma} (\nabla \cdot P_\gamma + \rho_\gamma g \nabla \cdot z) \quad (5)$$

242 where, $\bar{q}_\gamma [\text{m}^3 \text{s}^{-1}]$ is the Darcy flux, $K_{r\gamma}[-]$ is the relative permeability of the corresponding phase, $\nabla \cdot P$
 243 $[\text{Nm}^{-3}]$ is the driving force, $K [\text{m}^2]$ is intrinsic permeability of the medium, $\mu_\gamma [\text{kg m}^{-1} \text{s}^{-1}]$ is the viscosity
 244 of the corresponding fluid phase, and $\nabla \cdot z [-]$ is the upward unit vector.

245

246 The average saturation of the wetting and non-wetting phases in the domain are related as below,

$$247 S_w + S_{nw} = 1 \quad (6)$$

248

249 The P^c - S relationships are governed by the Brooks-Corey formulations (Brooks and Corey, 1964) as below,

$$250 S_{ew} = \left(\frac{P^c}{P^d} \right)^{-\lambda} \quad \text{for } P^c \geq P^d \quad (7)$$

$$251 S_{ew} = 1 \quad \text{for } P^c \leq P^d \quad (8)$$

$$252 S_{ew} = \left(\frac{S_w - S_{rw}}{1 - S_{rw}} \right) \quad \text{for } 0 \leq S_{ew} \leq 1 \quad (9)$$

253 where, $S_{ew} [-]$ the effective wetting phase saturation, $P^d [\text{Nm}^{-2}]$ is entry pressure, $\lambda [-]$ is pore size distribution
 254 index and $S_{rw} [-]$ is irreducible wetting phase saturation.

255

256 The relative permeabilities, K_{rn} and K_{rnw} , of the wetting and non-wetting phases in the domain are governed by
 257 the following Brooks-Corey-Burdine formulae (Brooks and Corey, 1964),

$$258 \quad K_{rw} = S_{ew}^{(2+\lambda)/\lambda} \quad (10)$$

$$259 \quad K_{mww} = (1 - S_{ew})^2 (1 - S_{ew}^{(2+\lambda)/\lambda}) \quad (11)$$

260

261 **2.2 Averaging Methods for Capillary Pressure Curves**

262 The averaging methods for capillary pressure data are discussed briefly in this section. The main assumption of
 263 our simulations/averaging methods is that we do not include any term for the effects of fluid/fluid interfacial
 264 area and common lines (see e.g., Murdoch and Hassanizadeh, 2002) on the macroscopic flow behaviour in
 265 porous media, as traditionally done for the extended version of Darcy's law for multiphase flow problem under
 266 steady-state condition. Theories have been proposed that allow inclusion of these effects on the macroscopic
 267 two-phase flow behaviour (e.g., Murdoch and Hassanizadeh, 2002). However, these are not trivial to
 268 implement in the type of continuum scale simulations carried out in this paper. It is perhaps more
 269 straightforward to include these effects in pore scale models (e.g., Held and Celia, 2001). However we note
 270 that our approach is consistent with most studies on dynamic effects at the macro-scale, which do not include
 271 effects of the fluid/fluid interfacial and common lines exclusively (Hassanizadeh et. al., 2002; Manthey et. al.,
 272 2005; O'Carrol et. al., 2005; Oung et. al., 2005; Berentsen et. al., 2006; Bottero et. al., 2006).

273

274 In our approach, the average capillary pressure and water saturation are calculated after each time step for both
 275 steady state and dynamic capillary pressure curves. These are based on the saturation-weighted average of fluid
 276 pressures in individual nodes in the domain, as below,

$$277 \quad \text{Saturation Weighted Average of } P^c: P^c \Big|_{t_n} = \langle P_{nw} \rangle \Big|_{t_n} - \langle P_w \rangle \Big|_{t_n} = \frac{\sum_{j=1}^m (1 - S_{wj}) P_{nwj}}{\sum_{j=1}^m (1 - S_{wj})} - \frac{\sum_{j=1}^m S_{wj} P_{wj}}{\sum_{j=1}^m S_{wj}} \quad (12)$$

278 where, t_n [s] is an arbitrary n^{th} time step, $\langle P_{nw} \rangle \Big|_{t_n}$ and $\langle P_w \rangle \Big|_{t_n}$ [Nm^{-2}] are the volume averaged non-wetting
 279 and wetting phase pressure, P_{nwj} and P_{wj} [Nm^{-2}] are the non-wetting and wetting phase pressures, and
 280 S_{nwj} and S_{wj} [-] are the saturation corresponding to non-wetting or wetting phase pressure at time t_n in an
 281 arbitrary j^{th} node where $j=1, 2, 3, \dots, m$, m being the total number of nodes in the domain.

282

283 At each node of the numerical grid, the saturation and volume of the wetting and non-wetting fluids are related
 284 as follows,

$$285 \quad V_{wj} + V_{nwj} = \phi \times V_j \quad (13)$$

$$286 \quad S_{w\gamma} = \frac{V_{\gamma j}}{V_j \times \phi}, \quad \gamma \equiv w, nw \quad (14)$$

$$287 \quad S_{wj} + S_{nwj} = 1 \quad (15)$$

288 where, V_{wj} , V_{nwj} and V_j are the volumes of the wetting and non-wetting phases in the 3D cell centred around
 289 the arbitrary node j , respectively. S_{nwj} is the saturation of the non-wetting phase at node j .

290

291 Average water saturation in the domain is calculated using an averaging of saturation of individual node in the
292 whole domain,

293 Average Saturation:
$$S_w \Big|_{t_n} = \frac{\sum_{j=1}^m S_{wj} V_j \Big|_{t_n}}{\sum_{j=1}^m V_j} \quad (16)$$

294 Based on the averaged water saturations at different time levels, the time derivative of saturation ($\partial S / \partial t$) is then
295 calculated, which is the slope at a point given by average water saturation and time level on a S-t curve. It is
296 approximated based on a central differencing scheme, as shown below,

297 The time derivative of saturation:
$$\frac{\partial S}{\partial t} \Big|_{S_w, t_n} = \frac{S_w \Big|_{t_{n+1}} - S_w \Big|_{t_{n-1}}}{t_{n+1} - t_{n-1}} \quad (17)$$

298 where, $S_w \Big|_{t_{n+1}}$ is the average wetting phase saturation at time step ‘ $n+1$ ’ calculated after the equation (16).

299

300 2.3 Simulator Used

301 The two-phase flow simulations have been carried out using the simulator STOMP (Subsurface Transport Over
302 Multiple Phases). The code is developed by the Pacific Northwest National Laboratory, US (www.pnl.gov) and
303 is capable of simulating 11 different modes of multiphase flow and multi-component transport in porous
304 media. In this case, we use the Water-Oil mode to simulate the dynamic and steady state two-phase flow
305 behaviour. STOMP has been successfully validated and applied to model a variety of multiphase flow
306 problems (e.g., Scroth et. al., 1998; Oostrom and White, 1998; Oostrom et. al., 1997; Ataie-Ashtiani et. al.,
307 2001, 2002; Das et. al., 2004, 2006). Ataie-Ashtiani et. al. (2001) have demonstrated the applicability of
308 STOMP to model flow of DNAPL and water in 2D heterogeneous domain by simulating a multi-fluid
309 laboratory experiment described by Kueper and Frind (1989). The spatial discretisation of the governing
310 equations is done based on the standard finite volume method, FVM (Patankar, 1980; Versteeg and
311 Malalasekera, 1995). The discretised equations are described in detail by White and Oostrom (2000). The
312 system of algebraic equations derived through the FVM discretisation of the governing equations and the
313 constitutive equations for P^c - S - K_r relationship involve non-linear terms. These non-linear equations are
314 reduced to linear forms by the application of the Newton-Raphson iterative methods for multiple variables. The
315 temporal discretisation is based on the implicit time stepping method.

316

317 2.4 Descriptions of Porous Media, Fluids Properties and Domains Geometries

318 Properties of fine and coarse sand, including intrinsic permeability, porosity, Brooks–Corey–Burdine
319 parameters along with the fluid properties are listed in Table 1. Figure 1 displays a heterogeneous domain
320 including 3D cylindrical column and, 2D and 3D rectangular domains. As discussed later, these domains are
321 used to determine the effects of domain geometries on the dynamic coefficient. The dimensions of these
322 domains are also shown in Figure 1.

323

324 **2.5 Initial and Boundary Conditions for Numerical Simulations**

325 There are two main laboratory methods of P^c - S - K_r measurements, namely, the flow-through and pressure-cell
326 experiments (Osoba et. al., 1951; Johnson et. al., 1959; Ataie-Ashtiani et. al., 2002). Our simulations
327 correspond to the pressure cell experiments for determining drainage P^c - S - K_r relationships. In these
328 experiments, the porous sample is made fully saturated with water and placed inside a reservoir filled with a
329 non-wetting phase. In our case we use PCE as the non-wetting phase, a common DNAPL contaminant found in
330 the subsurface. We apply constant pressure for PCE flow and ‘no flow’ boundary condition (BC) for water at
331 the top of the domain. ‘No flow’ BCs for both phases are imposed on the side of the domain. At the bottom
332 boundary of the domain, constant pressure for water and ‘no flow’ BC for PCE is applied. The outflow is
333 defined to be leveled with the top of the domain. This allows only water to drain out and overcomes free
334 downward flow of water. An example BC at the top and bottom of a 3D domain for different cases of dynamic
335 displacement of water by PCE is presented in Table 2. All simulations are carried out in the vertical direction
336 (downward displacement aligned with gravity) and therefore the gravity effects are included in all simulations.
337 However, we do not attempt to synthesize the gravity effects exclusively on the dynamic coefficient in this
338 paper.

339

340 **2.6 Quasi-static and Dynamic Two-phase Flow in Porous Media**

341 A series of dynamic and steady-state downward (along gravity) displacement experiments are simulated
342 involving water as wetting and PCE as non-wetting phase. In all simulations, PCE infiltrates at the top of either
343 3D cylindrical column or 2D and 3D rectangular domains initially fully saturated with water. The domain is
344 composed of either fine or coarse sand for homogeneous domains. Heterogeneous domains are represented by
345 binary combinations of small fine sand blocks imbedded in background coarse sand.

346

347 The procedure for simulating quasi-static displacement is as follows. The initial pressure of PCE is defined to
348 be zero everywhere. Then, the pressure of the non-wetting phase on the boundary of injection is gradually
349 increased. This leads to an increase in average capillary pressure, P^c . Once P^c reaches the entry pressure (P^d) of
350 the background medium, PCE infiltrates the sample and displaces water. The simulation is carried out until
351 steady-state flow conditions are reached, that is, saturation at all grid points does not vary any more with time
352 or this variation is smaller than a tolerance limit (10^{-6} in this case). The calculated average saturation and P^c
353 provide one point of the P^c - S curve. Next, the imposed PCE pressure is increased and the simulation is
354 continued until a new steady state is reached. A second point for P^c - S curve is thus obtained. This procedure is
355 repeated until a P^c of 11000 Pa is reached by which point the sample is deemed to have reached its irreducible
356 wetting phase saturation (S_{iw}).

357

358 For simulating dynamic two-phase flow behaviour, the imposed PCE pressure at the top of domain is increased
359 to a high pressure once and drainage takes place until the domain reaches its S_{iw} . We carry out simulations for
360 only drainage. Then, dynamic and steady state P^c - S curves for homogeneous and various heterogeneous
361 domains are prepared.

362

363 **2.7 Determination of Dynamic Coefficient (τ)**

364 Equation (2) shows that if $P^{c,dyn}$, $P^{c,equ}$ and time derivative of saturation ($\partial S / \partial t$) are known at a given saturation
365 value, the damping coefficient (τ) for a given sample can be determined. To obtain these data simulations
366 corresponding to ‘pressure cells’, often used for the measurement of P^c -S- K_r curves, are carried out for both
367 steady-state and dynamic two-phase flow in homogeneous and heterogeneous domains. The average values of
368 $P^{c,dyn}$, $P^{c,equ}$ and $\partial S / \partial t$ are determined as described in section 2.2. The averaged data are then used to calculate the
369 values of $(P^{c,dyn} - P^{c,equ})$ and $\partial S / \partial t$ for different cases and fitted to a straight line, if possible. The slope of this
370 straight line is then defined as the dynamic coefficient (τ) for that particular case. The initial and boundary
371 conditions for these simulations are described in section 2.5.

372

373 **2.8 Convergence of Numerical Results**

374 The grid size used in our simulations for 2D and 3D rectangular and 3D cylindrical domains are shown in
375 Table 3. In general, the convergence of the numerical solution is achieved based on a maximum Newton
376 iteration of either 16 or 32, depending on the complexity of the domain type and a tolerance limit of 10^{-6} .
377 However, we have also checked the convergence of the results through grid refinement. The results showed
378 that the grid refinement has negligible effects on the resultant P^c -S curves. For this test, the normal grid with 24
379 cells in Z-direction (Table 3) is refined four fold to include 96 cells in the domain whilst the domain size was
380 the same in all cases. The values chosen for $\Delta\Theta$ (nodal spacing in Θ direction) and Δr (nodal spacing in
381 r direction) are kept the same which is a reasonable assumption since the dominant direction of flow is in the
382 Z-direction and not in r - or Θ - directions. The P^c -S relationships for the normal (Table 3) and the refined grid
383 are then compared. The comparison shows negligible dependence of the P^c -S curves on the chosen grid. The
384 maximum percentage difference of $\sim 1.5\%$ is found between the P^c -S curves from the two cases. This gives
385 confidence that the results presented in this paper are, in general, independent of the grid size used and the
386 numerical results converge.

387

388 **3. Results and Discussion**

389

390 **3.1 Validity/Applicability of Equation (2) to Two-phase Flow in 3D Heterogeneous Porous Media**

391 In this section, we discuss the validity/applicability of equation (2) to dynamic two-phase flow in 3D porous
392 media with micro-scale heterogeneities. For these purposes, we have derived static and dynamic P^c -S curves for
393 various cases as discussed in section 2.6. Figure 2, for example, displays the dynamic and equilibrium capillary
394 pressure curves for homogeneous fine sand (3D cylindrical domain). Plots between the difference in dynamic
395 and equilibrium capillary pressure $(P^{c,dyn} - P^{c,equ})$ versus the time derivative of saturation ($\partial S / \partial t$) at certain
396 water saturation values are shown in Figures 3(a-c). These figures are then used to determine the dynamic
397 coefficient (τ) for various homogeneous and heterogeneous domains. Such plots, according to equation (2),
398 should represent a linear relationship passing through the origin. The slopes of these lines give the damping

399 coefficient, τ . The results as displayed in Figures 3(a-c) reveal that the linear functions do not necessarily run
400 through the origin and there is an intercept. Further, there is no clear dependence of the intercept term on either
401 the flow conditions or fluid and porous medium properties. The linear equations of the dynamic capillary
402 pressure relationships are directly shown in the figures, which indicate the dynamic coefficient (slope of the
403 straight line) and the intercept.

404

405 It seems from our results that the dynamic capillary pressure relationships may not be applicable in certain
406 range of saturations in pressure cells for measurement of two-phase flow properties. In other words, in these
407 cases it may not be possible to fit the data for $(P^{c.dyn} - P^{c.equ})$ and $\partial S / \partial t$ to a straight line with reasonable
408 accuracy. For example, as shown in Figure 3(d), at higher value of water saturation in a homogeneous fine
409 sand media, another relationship in the form of a polynomial function may exist for dynamic capillary
410 pressure. We observe that in general as the average value of water saturation and/or $\partial S / \partial t$ term decrease, the
411 degree of fitness of the data to a straight line increases. In other words, the applicability of equation (2)
412 increases with decrease in average water saturation and/or $\partial S / \partial t$ involving both homogeneous and
413 heterogeneous porous media. This needs to be investigated thoroughly and parameters for polynomial
414 functions for dynamic capillary pressure, if exist, need to be determined and interpreted in terms of two-phase
415 flow parameters in porous media. In this paper, we report values of dynamic coefficient for those ranges of
416 saturations where we obtain reasonable fit of equation (2) to a straight line.

417

418 **3.2 Material Properties Effects on Dynamic Coefficient**

419 In most natural porous media, the material properties, e.g., porosity, permeability, pore size distribution, entry
420 pressure etc., are correlated. It therefore makes more practical sense to synthesise the coupled effects of these
421 parameters on the dynamic coefficient rather than considering the effects of one variable at a time while
422 keeping other variables constant. In this section, we consider the material properties of homogeneous coarse
423 and fine sand as described in Table 1. We have conducted simulations for both dynamic and steady state two-
424 phase flow for these material properties. The applied boundary conditions to measure either dynamic or quasi-
425 static capillary pressure are the same for both sand types whilst the displacement time may vary. As expected, a
426 comparison of the P^c - S curves indicates higher irreducible water saturation and capillary pressure at the same
427 saturation in fine sand than those in coarse sand. This is due to higher capillary effect in smaller pores in fine
428 sand compared to coarse sand. This results in higher entrapped (end-point) saturation. Also, time derivative of
429 saturation ($\partial S / \partial t$) in dynamic flow in fine and coarse sand domain varies for the same boundary pressure.

430

431 Calculated dynamic coefficient as a function of the average water saturation for fine and coarse sand domains
432 are shown in Figure 4. The figure shows that the dynamic coefficient is a nonlinear function of the average
433 water saturation and increases as saturation decreases. This is consistent with recent works on determination of
434 dynamic coefficients. However, Figure 4 also indicates that for lower permeability and pore size distribution
435 index (λ), as in fine sand, the dynamic coefficient is significantly higher at the same water saturation. This
436 implies that the flow equilibrium is reached slower in these media. The main reason for this is higher capillary

437 pressure and lower Darcy velocity for individual fluid phase in fine sand. It takes longer time to drop to the
438 same water saturation in fine sand. Therefore, the time derivative of saturation is smaller in fine sand whilst the
439 difference between dynamic and static capillary pressure curves is almost the same to those in coarse sand (see,
440 e.g., Figure 3(a)). This leads to higher dynamic coefficient values in fine sand domains.

441

442 **3.3 Micro-heterogeneity Effects on Dynamic Coefficient**

443 Most laboratory and numerical experiments for the measurements of multiphase flow properties are conducted
444 on homogeneous domains. However, micro-heterogeneities with their distinct multiphase flow behaviour exist
445 in almost every core plug used to conduct these studies. Mantney et. al. (2005) performed numerical two-phase
446 flow displacement in spatially correlated random field of heterogeneity in a 2D rectangular domain. Das et. al.
447 (2006) also investigated effects of random distributions of heterogeneities in 2D rectangular domains on
448 capillary pressure curves without calculating the dynamic coefficient. None of these domain geometries are
449 comparable to real 3D cylindrical core plugs although these studies provide understanding of certain effects. It
450 is therefore not clear if the values of dynamic coefficient obtained for 2D heterogeneous domains may be used
451 directly for 3D heterogeneous cylindrical domains.

452

453 To address these issues, we apply a range of PCE pressures to homogeneous and heterogeneous cylindrical
454 domains (3D) with size comparable to those of laboratory core plugs to investigate micro-heterogeneity effects
455 on the dynamic coefficient. The proportion of fine sand lenses embedded in the coarse sand defines the
456 intensity of micro-heterogeneity (ω), as discussed before in section 1.4. Intensity and distribution of the
457 heterogeneities are varied in different heterogeneous domains. Soil heterogeneities in the form of variations in
458 intrinsic permeabilities (K) and/or entry pressure (P^d) affect the P^c - S curves and hence, the dynamic
459 coefficient. See for example Figures 5(a-b), which display two patterns with different intensities and
460 distributions of micro-heterogeneities within 3D cylindrical domains on $r - \Theta$ and $r - Z$ planes.

461

462 In Figures 6(a-d), we show the quasi-static and dynamic P^c - S curves for homogeneous and heterogeneous
463 media for various applied PCE pressures whilst water pressures at domain boundaries remain constant. As
464 expected, the results indicate that the presence of heterogeneity has a significant influence on the effective P^c - S
465 curves compared to the curves for homogeneous porous domains. Figures 6(b-d) show that as the PCE pressure
466 increases, the effective capillary pressure in the domain also increases at a given water saturation value.
467 However, as evident from the dynamic capillary pressure curves, dynamic effects become more prominent at
468 higher PCE pressure (Figure 6(d)). Furthermore, both steady state and dynamic P^c - S curves for heterogeneous
469 media lie between the P^c - S curves for homogeneous coarse and fine sand. Irreducible water saturation in
470 heterogeneous domains is higher than coarse sand and less than that of fine sand. These results are consistent
471 with other studies, which aim to synthesise micro-heterogeneity effects on two-phase flow behaviour (e.g.,
472 Ataie-Ashtiani et. al., 2001; Das et. al., 2004, 2006). Most of these studies show that micro-heterogeneities
473 have complex effects on the dynamics of the two-phase flow system. This is discussed below briefly as this
474 enables us to explain our results clearly.

475

476 For any value of intensity of heterogeneity, once the boundary pressure for PCE overcomes the entry pressure
477 of the domain, the PCE starts to infiltrate into the domain. The high density and low viscosity of PCE helps it
478 to flow downwards and drain water out of the domain. Contrast in permeability is important under dynamic
479 conditions because even small variations play a major role in determining the PCE distribution in the
480 heterogeneous sample. The fine sand lenses deflect the downward flow front of PCE because of their low
481 permeability. However, they do not have sufficient lateral extent to serve as a significant barrier to downward
482 flow of PCE. Wherever fine sand blocks are present, they cause local horizontal spreading of PCE at the top of
483 fine sand lenses. However, PCE finds its flow pathway around higher permeability regions and flows
484 downward in coarse background sand. Pools of PCE at the top of fine grained sand and, water trapped in fine-
485 grained sand blocks have a lot of interactions with flowing PCE in coarser background sand. Both PCE pools
486 and trapped water behave as an obstruction to PCE flow and water displacement. Because of PCE presence
487 around the fine sand blocks and eventually higher non-wetting phase relative permeability, the relative
488 permeability of water decreases dramatically. This causes water to remain in low permeability layers until the
489 pooled PCE pressure reaches the fine sand entry pressure and invades fine sand region. When this happens,
490 PCE displaces some of the trapped water in fine sand layers. Many small pools in discontinuous lenses are also
491 formed and in some cases it cannot be displaced because of lower relative permeability of wetting phase. These
492 results in a complex PCE distribution across the domain and consequently different effective capillary pressure
493 curves are obtained depending on the intensity and distribution of heterogeneities (Das et. al., 2006). Capillary
494 forces in any low permeability porous medium that PCE can enter trap a certain amount of water as residual
495 water.

496

497 As displayed in Figures 6(b-d), the trends (shape) of dynamic capillary pressure curves change at certain water
498 saturations and, the differences between the steady state and dynamic curves become significant. These figures
499 show that the difference becomes more prominent as the applied boundary PCE pressure increases. On the
500 other hand, this effect becomes less pronounced as the proportion of fine sand in the domain (intensity of
501 heterogeneity) increases and completely disappears in case of capillary pressure curves for fine sand. These
502 discrepancies are because of the contributions of gravity/viscous forces, presence of Haines jumps (Haines,
503 1930; Das et. al., 2006), and in situations when the PCE overcomes the entry pressure of fine sand to displace
504 the entrapped water in fine sand layers. In homogeneous fine sand with low permeability the humps are not
505 seen since there are no heterogeneities.

506

507 Using the procedures outlined in section 2.2, we have calculated dynamic coefficients (τ) for homogeneous and
508 heterogeneous domains at different water saturations (S) to quantify the micro-heterogeneity effects on the
509 dynamic coefficient. Our results on τ - S relationships are presented in Figures 6(a-d). In these figures, the
510 intensity of heterogeneity (ω) increases with increasing the proportion of fine sand lenses embedded in the
511 coarse sand domain. Higher intensity of heterogeneity results in a higher amount of entrapped water in the fine
512 sand blocks at the same boundary conditions. Therefore, the time derivative of saturation for the same

513 difference in dynamic and static capillary pressure ($P^{c,dyn} - P^{c,eq}$) is less at the same average water saturation
514 in the domain. This results in higher values of dynamic coefficient as the intensity of heterogeneity increases.

515

516 Our results show that as ω increases, the difference in the dynamic and equilibrium capillary pressure curves
517 increases. This also yields higher dynamic coefficient values at higher ω as shown in Figure 7. The figure
518 shows that contrary to homogeneous domains, the inclusion of heterogeneity significantly affects the dynamics
519 of the two-phase flow behaviour in porous media. However, one should not consider the intensity of
520 heterogeneity effect alone since the distribution and location of heterogeneity in the domain with respect to the
521 distance from infiltration also affects the PCE flow (Das et. al., 2004, 2006). For example, consider the
522 distributions of heterogeneities displayed in Figure 5(a-b). They result in different dynamic coefficients at the
523 same saturations for any given PCE pressure.

524

525 **3.4 Domain Geometry Effects on Dynamic Coefficient**

526 As discussed before, it is difficult to make a reliable prediction about the domain geometry effects on the
527 dynamic coefficient based on the reported data in the literature. This is because while there are differences in
528 the domain geometry and size used by various authors, there are also discrepancies in other parameters that
529 affect τ , e.g., material and fluid properties, boundary conditions, etc. To address this issue, we have carried out
530 a systematic study to synthesise the domain geometry effects on τ -S relationships for the same BCs, fluid, and
531 porous medium properties. We have performed simulations for vertically downward flow in both homogeneous
532 and heterogeneous 2D and 3D rectangular and 3D cylindrical domains (Figure 1). Fluid and porous medium
533 properties are the same (Table 1) in all domains. Heterogeneous domains imply binary combination of fine
534 sand and coarse sand. The intensity of heterogeneity in various geometries (e.g., 2D rectangular and 3D
535 domain) is kept the same. This enables us to make a reasonable comparison and explore geometry effects on
536 dynamic coefficient in both homogeneous and heterogeneous media.

537

538 As shown in Figure 8(a) and Figure 8(b), the shapes of P^c -S curves from cylindrical domains under dynamic
539 and steady state flow conditions, respectively, are similar to those obtained in 2D and 3D rectangular domains
540 although they are located slightly higher in the dynamic cases. This is due to the dimensionality effect on
541 dynamic fluid flow and saturation distribution in the cylindrical domain, which consequently affects the P^c -S
542 curves.

543

544 Figure 9 displays the dynamic saturation versus time for different domain geometries for homogeneous fine and
545 coarse sand. As evident, the time period to reach irreducible wetting-phase saturation increases in fine sand of
546 all geometries. This time duration in coarse sand is less than 6 hours for all domain geometries as shown in the
547 magnified profile in Figure 9. In fine sand, it is found to be more than 1000 hours regardless of domain
548 geometries. This is clearly due to water entrapment in smaller pore spaces and low permeability of fine sand.
549 Entrapment of fluid in smaller pores, strong attachment of the wetting fluid to the grain particles and difficulty
550 in displacing the wetting phase due to phase fragmentation are likely to affect saturation distribution in the

551 domain. Because of these phenomena, there are more interactions between fluid and porous media in fine-
552 grained domains. These affect the effective capillary pressure curves and, hence, the dynamic coefficient.

553

554 The τ -S relationships for both homogeneous and heterogeneous 2D rectangular domain and 3D cylindrical
555 columns are discussed here to show if domain geometry has any effect on the dynamic coefficient (Figure 10).
556 Our results show that 3D cylindrical domain results in slightly higher dynamic coefficient values as compared
557 to those values for 2D rectangular domain, at the same saturation. But this difference is negligible in
558 homogeneous domains. This implies that the inconsistencies in dynamic coefficient values are less likely to be
559 caused by geometry if the porous domains are homogeneous and isotropic with respect to material properties
560 (e.g., permeability). However, the differences in the dynamic coefficient values for 2D and 3D heterogeneous
561 domains are more pronounced. This is clearly an effect of the presence of heterogeneities in the domain. For
562 example, the heterogeneities may cause lateral spreading of PCE and entrapment of fluid in the fine sand
563 blocks (Ataie-Ashtiani, et. al., 2001; Das et. al., 2004, 2006). This results in higher dynamic coefficient at the
564 same saturation, as we show in Figure 10.

565

566 **3.6 Permeability Anisotropy Ratio Effects on Dynamic Coefficient**

567 While formulating his law, Darcy defined the permeability to be the same in all directions (Darcy, 1856).
568 However, this is hardly the case ever and anisotropy in permeability frequently occurs in natural porous media
569 in different directions. For example, anisotropy may appear where the soil has deposited in different layers. In
570 many cases, the soil grains have preferred orientations depending on depositional environments, which create
571 anisotropy in the media permeability. Therefore, core samples collected from the field for laboratory
572 experiments are expected to have anisotropy in permeability.

573

574 In this section, we aim to characterise the implications of anisotropy in permeability values on the dynamic
575 effects in both homogeneous and heterogeneous porous domains. For this purpose, we use a term anisotropy
576 ratio, which is defined as the ratio of the vertical permeability (K_v) to the horizontal permeability (K_h) in 3D
577 cylindrical domain. The ratio gives an indication of the permeability anisotropy, i.e., higher is the ratio higher
578 is the media anisotropy. For our simulations, we vary the ratios by varying vertical permeability while the
579 horizontal permeability is kept constant. Note that in all previous simulations, the anisotropy ratio was 1.0, i.e.,
580 the permeability values were the same in both horizontal and vertical directions within homogeneous media. In
581 heterogeneous media, there was a contrast in permeability values of 10^3 between coarse and fine sand. This
582 contrast in permeability is maintained in the heterogeneous domains that are defined for the purpose of this
583 section.

584

585 The effects of anisotropic ratio (K_v/ K_h) on the dynamic coefficient-saturation (τ -S) relationships are displayed
586 in Figure 11. We have chosen a homogeneous coarse sand domain (Table 1) and heterogeneous domain with
587 the intensity of heterogeneity of 0.207 to illustrate the effects of permeability anisotropy. As shown in the
588 figure, lower anisotropic ratio (i.e., lower permeability in vertical direction) results in higher dynamic

589 coefficient for a given saturation value, especially in heterogeneous domains. This is because the lower
590 permeability in vertical direction behaves as a barrier to the PCE flow and causes it's spreading in the
591 horizontal direction. This also implies slower PCE flow across the domain in vertical direction and larger
592 amount of entrapped water in the micro-heterogeneities in the domain. This results in slow water displacement
593 in the domain in the direction of imposed pressure gradient. Consequently, the equivalence between the static
594 and dynamic P^c-S curves is not established quickly for lower anisotropic ratio. This results in higher values of
595 dynamic coefficient at a given saturation when anisotropy ratio is smaller. When the anisotropy ratio is higher,
596 the reverse is observed, i.e., the dynamic coefficient at any given saturation becomes smaller.

597

598 In general, if the permeability anisotropy ratio (K_v/K_h) is small in the direction of fluid flow and/or imposed
599 pressure drop across the flow domain, the dynamic coefficient increases, and vice versa.

600

601 **3.7 Domain Aspect Ratio Effects on Dynamic Coefficient**

602 As discussed before, a number of authors have conducted laboratory and/or numerical two-phase flow
603 experiments in domains of different geometries and size where the material properties and BCs are not
604 necessarily the same. In many cases, the chosen domains have been simplified to address certain questions. It is
605 therefore difficult to make precise idea of the effects of varying domain size on the dynamic coefficient. To
606 address this issue, we have conducted numerical experiments on 3D cylindrical domains (both homogeneous
607 and heterogeneous) with varying aspect ratios (L/D). The effects of domain aspect ratios on the dynamic
608 coefficient are then assessed for three different values by changing the length (L) of the domain while the
609 diameter (D) is kept the same. In the case of the heterogeneous domains, we have kept the same distribution
610 and intensity of micro-heterogeneity. This makes sure that any difference in the results is because of the
611 change in the domain aspect ratio and not because of heterogeneity patterns. We have also kept the same BCs
612 in all cases. In general, BCs have significant effects on the dynamic coefficient (Manthey et. al., 2005).
613 However, we do not make attempt in this paper to address the coupled effects of BCs and aspect ratio on the
614 dynamic coefficients.

615

616 τ -S relationships in Figure 12 show that if the aspect ratio is higher (i.e., longer domain), the dynamic
617 coefficient is also higher for both homogeneous and heterogeneous domains at the same effective water
618 saturation. However, the increase in the dynamic coefficient in case of heterogeneous domain is much more
619 dramatic as compared to the homogeneous domains. In the case of longer samples, the distance for DNAPL
620 flow across the domain increases which increases the fluid-solid interactions and fluid residence time in the
621 domain. This results in higher dynamic coefficient values at the same water saturation provided the BCs
622 remain the same. Our results for 3D cylindrical domains qualitatively agree with most previous studies on
623 dynamic coefficient for 2D rectangular domains (flow through type cells), which indicate that the dynamic
624 coefficients increase with increase in domain size (Gielen et. al., 2005; Manthey et. al., 2005). However, we do
625 not compare our results (pressure cells) directly with these studied because of the difference in domain size
626 and geometry, type of flow cell and, boundary conditions used.

627

628 **4. Conclusions**

629 In this work, we have reported results of our numerical experiments for quasi-static and dynamic two-phase
630 flow in 2D rectangular and 3D cylindrical domains in vertical direction along gravity. The results show that the
631 linear relationship proposed in literature for dynamic capillary pressure is applicable for lower water saturation
632 when $\partial S/\partial t$ is small. However, a polynomial function may be more applicable at higher water saturation when
633 the $\partial S/\partial t$ term is higher. The parameters for these relationships (e.g., dynamic coefficients, $\partial S/\partial t$, etc) vary from
634 one case to another depending on many factors, e.g., flow parameters in porous media, domain shape and size,
635 intensity and distribution of heterogeneities, etc. Therefore, the significance of the parameters in the dynamic
636 capillary pressure relations needs to be determined and interpreted carefully in terms of those parameters to
637 apply these relationships in real life scenarios. The simulations carried out in this work provide range of
638 dynamic coefficient values in realistic cases.

639

640 Our results show that the non-uniqueness in P^c -S curves and discrepancies in dynamic coefficient are caused
641 not only by dynamic flow condition but also the nature, distribution, and intensity of micro-heterogeneity, pore
642 size distribution, domain size and geometry, and media anisotropy have their own effects. However, there is a
643 complex interplay of different variables. Cylindrical column used to simulate laboratory drainage seems to
644 result in similar P^c -S curves to 2D and 3D rectangular domains of equal volume. However, the dynamic
645 coefficient is different from one domain to another, especially in heterogeneous domains. This implies that the
646 dynamics of the flow depend on the geometry of the domain and the P^c -S relationships obtained for one
647 domain geometry may not be used directly for domain of different geometry. For example, in cases where P^c -S
648 relationships are upscaled from core scale to larger scales, one should pay particular attention to the shape of
649 the domain geometries in both core and larger scales. Our results also show that the P^c -S curves are subjected
650 to greater dynamic effects in heterogeneous domains.

651

652 For micro-heterogeneities of the type used in this study, as the intensity of heterogeneity increases the dynamic
653 coefficient increases. But this dependence is not a linear function and depends also on the distribution of
654 micro-heterogeneity. Values of dynamic coefficient obtained in this study are higher than most previously
655 reported values for the same domain size. However, this is plausible because we consider both 3D and micro-
656 heterogeneity effects in a dynamic flow condition.

657

658 **Acknowledgements**

659 This study has been carried in the framework of the EPSRC (UK) Project GR/S94315/01, “micro-heterogeneity
660 and temperature effects on dynamic capillary pressure-saturation relationships for two-phase flow in porous
661 media”. The EPSRC funding is gratefully acknowledged. Prof. S.M. Hassanizadeh at Utrecht University, the
662 Netherlands is a visiting professor on this project. Prof. Hassanizadeh is acknowledged for many fruitful
663 discussions on the subject. Comments of three anonymous referees, which helped to improve the clarity of the
664 paper, are sincerely acknowledged.

665

666 **References**

667 Ataie-Ashtiani, B., Hassanizadeh, S.M., Oostrom, M., Celia, M.A., White, M.D., 2001. Effective parameters
668 for two-phase flow in a porous medium with periodic heterogeneities. *J. Contaminant Hydrology* 49:87-109.

669

670 Ataie-Ashtiani, B., Hassanizadeh, S.M., Celia, M.A., 2002. Effects of heterogeneities on capillary pressure–
671 saturation–relative permeability relationships. *J. Contaminant Hydrol.*, 56(3-4): 175–192.

672

673 Avraam, D. G., Payatakes, A.C., 1995. Flow regimes and relative permeabilities during steady-state two-phase
674 flow in porous media. *Journal of Fluid Mechanics*, 293:207–236.

675

676 Barenblatt, G. I., Patzek, T. W., Silin, D. B., 2003. The mathematical model of non-equilibrium effects in
677 water-oil displacement. *SPEJ*, 84: 409-416.

678

679 Barenblatt, G.I., Entov, V.M., Ryzhik, V.M., 1990. Theory of fluid flows through natural rocks, Kluwer
680 Academic Publishers, Dordrecht, the Netherlands.

681

682 Bear, J., 1972. *Dynamics of fluids in porous media*. Dover Publications, New York.

683

684 Bear, J. and Verruijt, A., 1987. Modelling groundwater flow and pollution. D. Reidel Publ. Co., Dordrecht, the
685 Netherlands, 414 p.

686

687 Beliaev, A.Y., Hassanizadeh, S.M., 2001. A theoretical model of hysteresis and dynamic effects in the
688 capillary relation for two- phase flow in porous media. *J. Transp. Porous Media* 43: 487–510.

689

690 Beliaev, A.Y., Schotting, R.J., 2002. Analysis of a new model for unsaturated flow in porous media including
691 hysteresis and dynamic effects. *Computational geosciences*, 5: 345-368.

692

693 Berentsen, C.W.J., Hassanizadeh, S.M., Bezuijen, A, Oung, O. 2006. Modelling of two-phase flow in porous
694 media including non-equilibrium capillary pressure effects. Proceedings of the XVI International Conference
695 on Computational Methods in Water Resources (CMWR), Copenhagen, Denmark.

696

697 Blom, S.M.P., 1991. Relative permeability to near-miscible fluids. Delft University of Technology. Delft, The
698 Netherlands, 174 p.

699

700 Blunt, M., and King, P., 1991. Relative permeabilities from two- and three-dimensional pore-scale network
701 modeling. *J. Transp. Porous Media*, 6: 407- 433.

702

703 Bottero, S, Hassanizadeh, S.M., Kleingeld, Bezuijen, A., 2006. Experimental study of dynamic capillary
704 pressure effect in two-phase flow in porous media. Proceedings of the XVI International Conference on
705 Computational Methods in Water Resources (CMWR), Copenhagen, Denmark.
706

707 Bourgeat, A., Panfilov, M., 1998. Effective two-phase flow through highly heterogeneous porous media:
708 capillary non-equilibrium effects. *Computational Geosciences* 2: 191-215.
709

710 Brooks, R.H., and Corey, A.T., 1964. Hydraulic properties of porous media. *Hydrology Papers*. Colorado State
711 University.
712

713 Burdine, N. T., 1953. Relative permeability calculations from pore size distribution data. *Petroleum Trans.*
714 198: 71-77.
715

716 Collins, R.E., 1961. *Flow of Fluids through Porous Material*, Reinhold Publishing Corporation, New York.
717

718 Dahle, H.K., Celia, M.A., Hassanizadeh, S.M., 2005. Bundle-of-tubes model for calculating dynamic effects in
719 the capillary pressure-saturation relationship. *Transport in Porous Media*, 58(1-2): 5-22.
720

721 Darcy, H., 1856. *Les Fontaines Publiques de la Ville de Dijon*. Paris: Victor Dalmont.
722

723 Das, D.B, Hassanizadeh, S.M., Rotter, B.E., Ataie-Ashtiani, B., 2004. A numerical Study of Micro-
724 heterogeneity Effects on Upscaled Properties of Two-Phase Flow in Porous Media. *Transp. Porous Media*, 56:
725 329-350.
726

727 Das D. B., Mirzaei, M., Widdows, N., 2006. Non-Uniqueness in Capillary Pressure-Saturation-Relative
728 Permeability Relationships for Two-Phase Flow in Porous Media: Implications of Intensity and Random
729 Distribution of Micro-Heterogeneity. *J. Chem. Eng. Science*. 61: 6786-6803.
730

731 Davidson, J.M., Nielsen, D.R. and Biggar, J.W., 1966. The dependence of soil water uptake and release upon
732 the applied pressure increment. *Soil. Sci. Soc. Am. Proc.* 30: 298-304.
733

734 Delshad, M., Pope, G., Lake, L., 1987. Two- and three-phase relative permeabilities of micellar fluids. *SPE*
735 *Form. Eval.*, (Sept.), 327– 337.
736

737 DiCarlo, D.A. and Blunt, M.J., 2000. Determination of finger shape using the dynamic capillary pressure.
738 *Water Resources Research* 36(9): 2781-2785.
739

740 Fulcher, R. A., Ertekin, T., and Stahl, C. D., 1985, Effect of capillary number and its constituents on two-phase
741 relative permeability curves, *J. Petrol. Tech.*, (Feb.), 249–260.

742

743 Gielen, A.J.M., Hassanizadeh, S.M., Nordhaug, H.F., Leijnse, A., 2005. Dynamic effects in multiphase flow: a
744 pore-scale network approach. In Das, D.B. and Hassanizadeh, S.M., 2005. Special issue on: Upscaling
745 multiphase flow in porous media: from pore to core and beyond. Springer, The Netherlands.

746

747 Haines, W.B., 1930. "Studies in the physical properties of soil the hysteresis effect in capillary properties and
748 the modes of moisture distribution associated therewith", *J. Agricultural Sci.*, **20**, 97-116.

749

750 Hanyga, A., Sereczynska, M., 2005. A **dynamic** model of capillary hysteresis in immiscible fluid displacement.
751 Transport in **Porous** Media, 59:249-265.

752

753 Hassanizadeh S.M., Celia, M.A., Dahle, H.K., 2002(a). Dynamic effect in the capillary Pressure- Saturation
754 and its impact on unsaturated flow. *Vadose Zone Hydrology*, 1: 38-57.

755

756 Hassanizadeh, S.M., Celia, M.A., Dahle, H.K., 2002(b). Dynamic effect in the capillary pressure – saturation
757 relationship and its impact on unsaturated flow. *Agricultural Sciences*, 7(2): 69-71.

758

759 Hassanizadeh, S.M., Gray, W.G., 1993(a). Thermodynamic basis of capillary pressure in porous media. *Water*
760 *Resources Research* 29(10): 3389-3405.

761

762 Hassanizadeh, S.M., Gray, W.G., 1993(b). Toward an improved description of the physics of two-phase flow.
763 *Adv. Water Resources*, 16: 53-67.

764

765 Helmig, R., 1997. *Multiphase flow and transport processes in the subsurface*. Springer, 367 P.

766

767 Henderson, G.D., Danesh, A., Al-kharusi, B., Tehrani, D., 2000. Generating reliable gas condensate relative
768 permeability data used to develop a correlation with capillary number. *J. Pet. Sci Eng.* 25, 79.

769

770 Hilfer, R., 1996. *Transport and Relaxation Phenomena in Porous Media*. *Adv. Chem. Phys.*, XCII: 299 – 424.

771

772 Illangasekare, T.H., Yates, T.H., Armbruster, E.J., 1995. Effects of heterogeneity on transport and entrapment
773 of nonequous phase waste products in aquifers: an experimental study, *ASCE J. of Env. Eng.*, 121(8): 572-579.

774

775 Illangasekare, T.H., Ramsey, J.L., Jensen, K.H., Butts, M., 1995. Experimental study pf movement and
776 distribution of dense organic contaminants in heterogeneous aquifers, *J. of Contaminant Hydrology*, 20: 1-25.

777

778 Johnson, E.F., Bossier, D.P., Naumann, V.O., 1959. Calculation of Relative Permeability from
779 Displacement Experiments. *Trans.AIME.*, 370,216.

780
781 Kalaydjian, F. 1992. Dynamic capillary pressure curve for water/oil displacement in porous media: theory vs.
782 experiment. SPE Paper 24813. SPE Conference. Washington, DC. USA.
783
784 King, P.R., 1989. The Use of Renormalization for Calculating Effective Permeability. *Transp. Porous Media*,
785 4: 37-58.
786
787 Kueper, B.H., Frind, E.O., 1991. Two-phase flow in heterogeneous porous media 1. Model development.
788 *Water Resources Rs.* 27: 1049–1057.
789
790 Kueper, B.H., Frind, E.O., 1989. An overview of immiscible fingering in porous media. *J. Contam. Hydrol.* 5:
791 83-95.
792
793 Kueper, B.H., McWhorter, D.B., 1991. The behavior of dense, nonaqueous phase liquids in fractured clay and
794 rock. *Ground Water*. 29(5): 716-728.
795
796 Leverett, M. C., 1939. Flow of oil–water mixtures through unconsolidated sands. *Trans. AIME* 132:149
797
798 Manthey, S., Hassanizadeh, S.M., Helmig, R., 2005. Macro-scale dynamic effects in homogeneous and
799 heterogeneous porous media, *Transp. Porous Media*, 58(1-2): 121-145.
800
801 Mirzaei, M., Gaudie, R., Das, D.B., 2006. Dynamic Effects in Two-phase Flow in Porous Media: Inclusion of
802 3D and Micro-scale Heterogeneities. *Proceedings of the XVI International Conference on Computational*
803 *Methods in Water Resources (CMWR)*, Copenhagen, Denmark.
804
805 Muskat, M., Mears, M., 1936. The flow of heterogeneous fluids through porous media, *Physics*.7 (346–363).
806
807 Nordbotten, J.M., Celia, M.A., Dahle, H.K., Hassanizadeh, S.M., 2006. On the definition of macro-scale
808 pressure for multiphase flow in porous media. *Proceedings of the XVI International Conference on*
809 *Computational Methods in Water Resources (CMWR)*, Copenhagen, Denmark.
810
811 O'Carroll, D.M., Phelan, T. J., Abriola, L.M., 2005. Exploring dynamic effects in capillary pressure in
812 multistep outflow experiments, *Water Resour. Res.*, 41, W11419, doi: 10.1029/2005WR004010.
813
814 Oostrom, M., Hofstee, C., Dane, J.H., 1997. Light nonaqueous-phase liquid movement in a variably saturated
815 sand. *Soil Science Society of America Journal*, 61, 1547–1554.
816

817 Oostrom, M., Lenhard, J., 1998. Comparison of relative permeability–saturation–pressure parametric models
818 for infiltration and redistribution of a light nonaqueous phase liquid in sandy porous media. *Advances in Water*
819 *Resources*, 21:145–157.

820

821 Osoba, J.S., Richardson, J.J., Kerver, J.K., Hafford, J.A., Blair, P.M., 1951. Laboratory Measurements of
822 Capillary Pressure and Relative Permeability. *Transactions, AIME*, Vol.192: 47-55.

823

824 Oung, O., Hassanizadeh, S.M., Bezuijen, A., 2005. Two-phase flow experiments in a geocentrifuge and the
825 significance of dynamic capillary pressure effect. *J. Porous Media*, vol. 8(3): 247-257.

826

827 Patankar, S.V., 1980. Numerical heat transfer and fluid flow. New York: Hemisphere, 197p

828

829 Porter, M.L., Schaap, M.G., Wildenschild, D., 2006. Capillary pressure-Saturation Curves: Towards
830 Simulating Dynamic Effects with the Lattice-Boltzman Method. Proceedings of the XVI International
831 Conference on Computational Methods in Water Resources (CMWR), Copenhagen, Denmark.

832

833 Scheidegger, A.E., 1974. *Physics of Flow Through Porous Media*. Toronto, University of Toronto Press.

834

835 Schuille, F., 1988. Dense Chlorinated Solvents in Porous and Fractured Media: Model Experiments. ed.
836 Chelsea, MI, Lewis Publishers, Inc. 146 pp.

837

838 Singh, M., Mohanty, K.K., 2003. Dynamic modelling of drainage through three-dimensional porous materials.
839 *Chemical Engineering Science*, 58: 1-18.

840

841 Stauffer, F., 1978. Time dependence of the relationship between capillary pressure, water content and
842 conductivity during drainage of porous media. In proceedings of the IAHR conference on scale effects in
843 porous media, Thessaloniki, Greece.

844

845 Theodoropoulou, M.A., Sygouni, V., Karoutsos, V., Tsakiroglou, C.D., 2005. Relative permeability and
846 capillary pressure functions of porous media as related to the displacement growth pattern *International*
847 *Journal of Multiphase Flow*, Volume 31, Issues 10-11: 1155-1180

848

849 Theodoropoulou, M.A., Karoutsos, V, Tsakiroglou, C., 2001. Investigation of the contamination of fractured
850 formations by non-Newtonian oil pollutants, *J. Environ. Forensics* 2:321–334

851

852 Tsakiroglou, C.D., Theodoropoulou, M.A., Karoutsos, V., 2003. Nonequilibrium Capillary Pressure and
853 Relative Permeability Curves of Porous Media. *AICHE Journal*, 49 (10), 2472-2486.

854

855 Tsakiroglou, C.D., 2004. Correlation of the two-phase flow coefficients of porous media with the rheology of
856 shear-thinning fluids, *J. Non-Newtonian Fluid Mech*, 117:1–23.

857

858 Topp, G.C., Klute, A., Peters, D.B., 1967. Comparison of water content-pressure head obtained by equilibrium,
859 steady-state and unsteady state methods. *Soil Sci. Amer. Proc.* 31: 312-314.

860

861 Vachaud, G., Vauclin, M., Wakil, M., 1972. A study of the uniqueness of the soil moisture characteristic
862 during desorption by vertical drainage, *Soil Sci. Soc. Amer. Proc.*, 36, 531–532.

863

864 Versteeg, H. K.; Malalasekera, W., 1995. An introduction to computational fluid dynamics - the finite volume
865 method. London, Longman Scientific and Technical, 257p

866

867 Wildenschild, D., Hopmans, J. W., Simunek, J., 2001., Flow rate dependence of soil hydraulic characteristics,
868 *Soil Sci. Soc. Amer. J.*, 65, 35–48.

869

870 Wildenschild, D., Hopmans, J.W., Rivers, M.L., Kent, A.J.R., 2005. Quantitative analysis of flow processes in
871 a sand using synchrotron x-ray microtomography. *Vadose Zone Journal* 4:112-126.

872

873 Whitaker, S., 1986. Flow in Porous Media II: the Governing Equations for Immiscible Two-Phase Flow.
874 *Transp. Porous Media*, 1, 105.

875

876 White, M.D., Oostrom, M., Lenhard, R.J., 1995. Modelling fluid-flow and transport in variably saturated
877 porous media with STOMP simulator: 1.Non-volatile 3-phase model description. *Advances in Water*
878 *Resources*, 18(6), 353-364.

879

880 www.pnl.gov

List of tables

Table-1: Model parameters used in simulation (adopted from Kueper and Frind, 1989; Ataie-Ashtiani et. al., 2001; Das et. al., 2004, 2006)

Table-2: Boundary condition for different dynamic drainage displacement cases for cylindrical domain sand sample.

Table-3: Number of nodes and nodal spacing for different domain geometries

List of figures

Figure 1. Representative domains geometry and dimensions used in simulations.

Figure 2. Steady-State and Dynamic Capillary Pressure Curves for Fine Sand Model.

Figure 3(a-d). Dynamic coefficient for (a) fine sand, (b) coarse sand, (c) heterogeneous sample with intensity of heterogeneity (ω) of 0.207, (d) fine sand at high saturations in cylindrical domain.

Figure 4. Pore size distribution (λ) and permeability (K) effects on dynamic coefficient (τ) value in a homogeneous cylindrical column consisting of either fine or coarse sand.

Figure 5(a-b). 3D cylindrical domains for two intensities (ω) and distributions of micro-heterogeneities in the form of sub-sample scale fine sand blocks (dark grey regions) embedded in coarse sand background: (a) $\omega=0.207$, and (b) $\omega=0.372$.

Figure 6(a-d). Micro-Heterogeneity effects on (a) Steady-State and, Dynamic P^c-S curves for PCE pressure of (b) 109316 Pa, (c) 112513 Pa, and (d) 122903 Pa applied at the Top of a cylindrical domain. All results are for downward flow of PCE in cylindrical domains (3D).

Figure 7. The effect of intensity of heterogeneity (ω) on dynamic coefficient (τ).

Figure 8. (a) Effective dynamic capillary pressure curves for coarse and fine sand domains and (b) effective steady-state capillary pressure curves for coarse sand in different domain geometries.

Figure 9. Saturation profile for coarse and fine sand considering different domain geometries under dynamic flow condition.

Figure 10. Domain geometry effect on dynamic coefficient; geometry slightly affects dynamic coefficient (τ) for flow in homogeneous coarse sand and heterogeneous domains for the geometries and dimensions shown in Fig. 1.

Figure 11. Effect of permeability anisotropy on dynamic coefficient for a homogeneous and heterogeneous domain with intensity of heterogeneity (ω) = 0.207 .

Figure 12. Effect of aspect ratio on dynamic coefficient for homogeneous and heterogeneous domains with intensity of heterogeneity (ω) = 0.331. Aspect ratio for cylindrical domain has been defined as Length/Diameter (L/D).

Table-1: Model parameters used in simulation (adopted from Kueper and Frind, 1989; Ataie-Ashtiani et. al., 2001; Das et. al., 2004, 2006)

Property	Coarse Sand	Fine Sand	Water	PCE (DNAPL)
Permeability, K (m^2)	5×10^{-9}	5×10^{-12}	-	-
Porosity, ϕ (-)	0.40	0.40	-	-
Displacement Pressure, P^d (Nm^{-2})	370	1325	-	-
Pore size distribution index, λ (-)	3.86	2.49	-	-
Irreducible Water Saturation, S_{iw} (-)	0.078	0.098	-	-
Density, ρ (kgm^{-3})	2630	2650	1000	1630
Viscosity, μ ($kgm^{-1}s^{-1}$)	-	-	1×10^{-3}	0.9×10^{-3}
Surface Tension, σ (Nm^{-1})	-	-	0.072^a	0.035^b

a- Water-air system

b- PCE-water system

Table-2: Boundary conditions for different dynamic drainage cases for sand sample in cylindrical domain in a pressure cell used for the measurement of two-phase flow properties. Dirichlet BCs of pressure are imposed for DNAPL at the Top and water at the Bottom. Zero flux BCs are imposed for water at the Top and DNAPL at the bottom. This allows only DNAPL infiltration at the Top and water outflow at the Bottom of the pressure cell.

Displacement case	Time Duration (hr)	Top Boundary		Bottom Boundary	
		Dirichlet DANPL Pressure (Pa)	Zero Flux Water	Dirichlet water Pressure (Pa)	Zero Flux DNAPL
Dynamic case-1	5.6	109316		102510	
Dynamic case-2	3.9	112513		102510	
Dynamic case-3	2.8	117308		102510	
Dynamic case-4	2.1	122903	102510		

Table-3: Number of nodes and nodal spacing for different domain geometries

Domain geometry	Number of nodes \times Nodal Spacing				
	$N \times \Delta r$ (cm)	$N \times \Delta \Theta$ (degree)	$N \times \Delta X$ (cm)	$N \times \Delta Y$ (cm)	$N \times \Delta Z$ (cm)
2D Rectangular	-	-	8×1.25	1×7.92	$1 \times 0.05, 24 \times 0.5, 1 \times 0.05$
3D Rectangular	-	-	8×1.25	8×0.988	$1 \times 0.05, 24 \times 0.5, 1 \times 0.05$
3D Cylindrical	4×1.25	4×90	-	-	$1 \times 0.05, 24 \times 0.5, 1 \times 0.05$

N : Number of nodes

Δr : Nodal Spacing in r direction for cylindrical domain

$\Delta \Theta$: Nodal spacing in Θ direction for cylindrical domain

ΔX : Nodal spacing in X direction for rectangular domain (2D or 3D)

ΔY : Nodal spacing in Y direction for rectangular domain (2D or 3D)

ΔZ : Nodal spacing in Z direction for rectangular domain (2D or 3D)

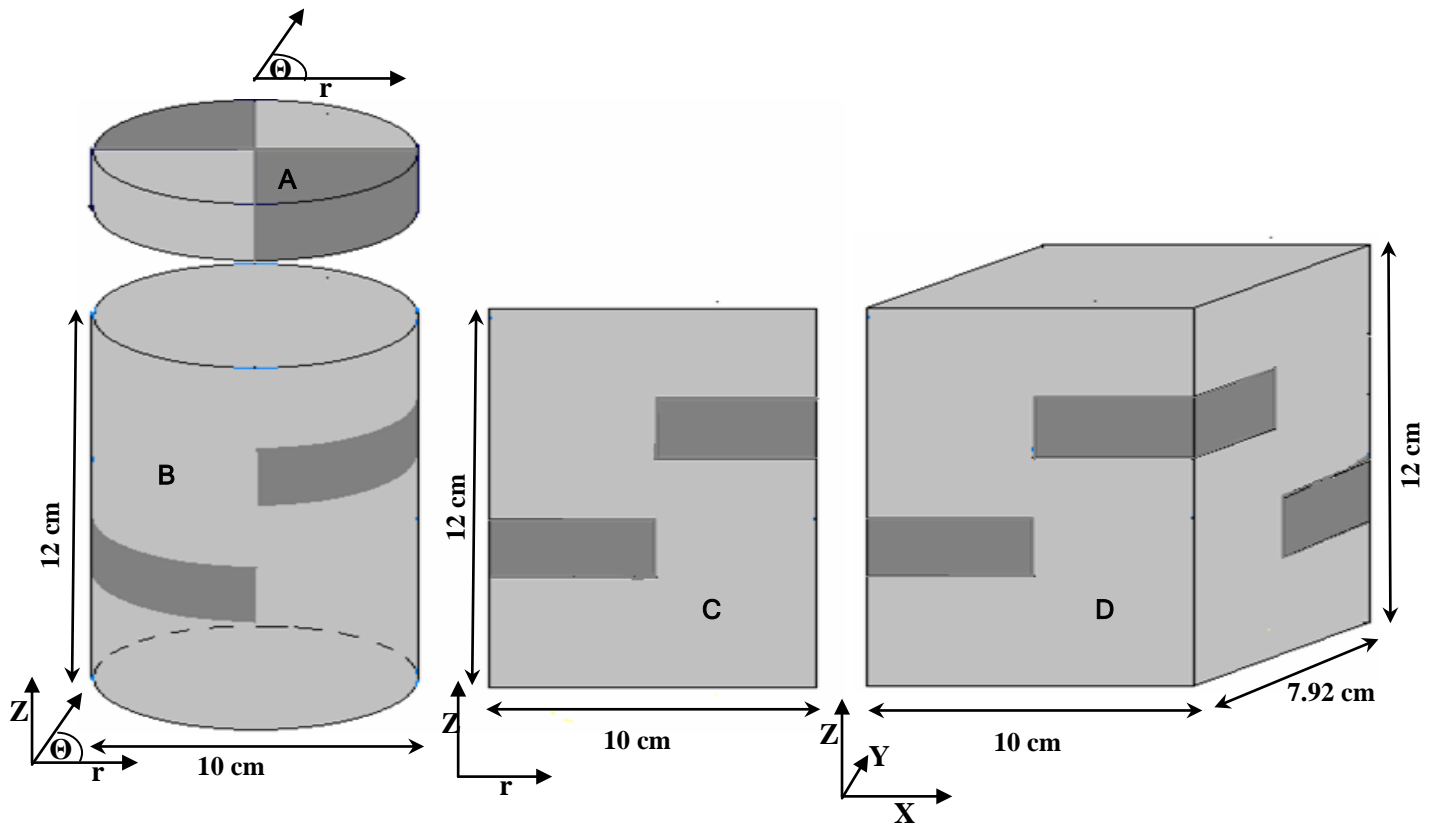


Figure 1. Representative domains used in simulations: (A) r - θ section of heterogeneity distribution, (B) 3D cylindrical domain geometry, (C) 2D $(r$ - $Z)$ section of heterogeneity in a cylindrical domain, (D) 3D rectangular domain.

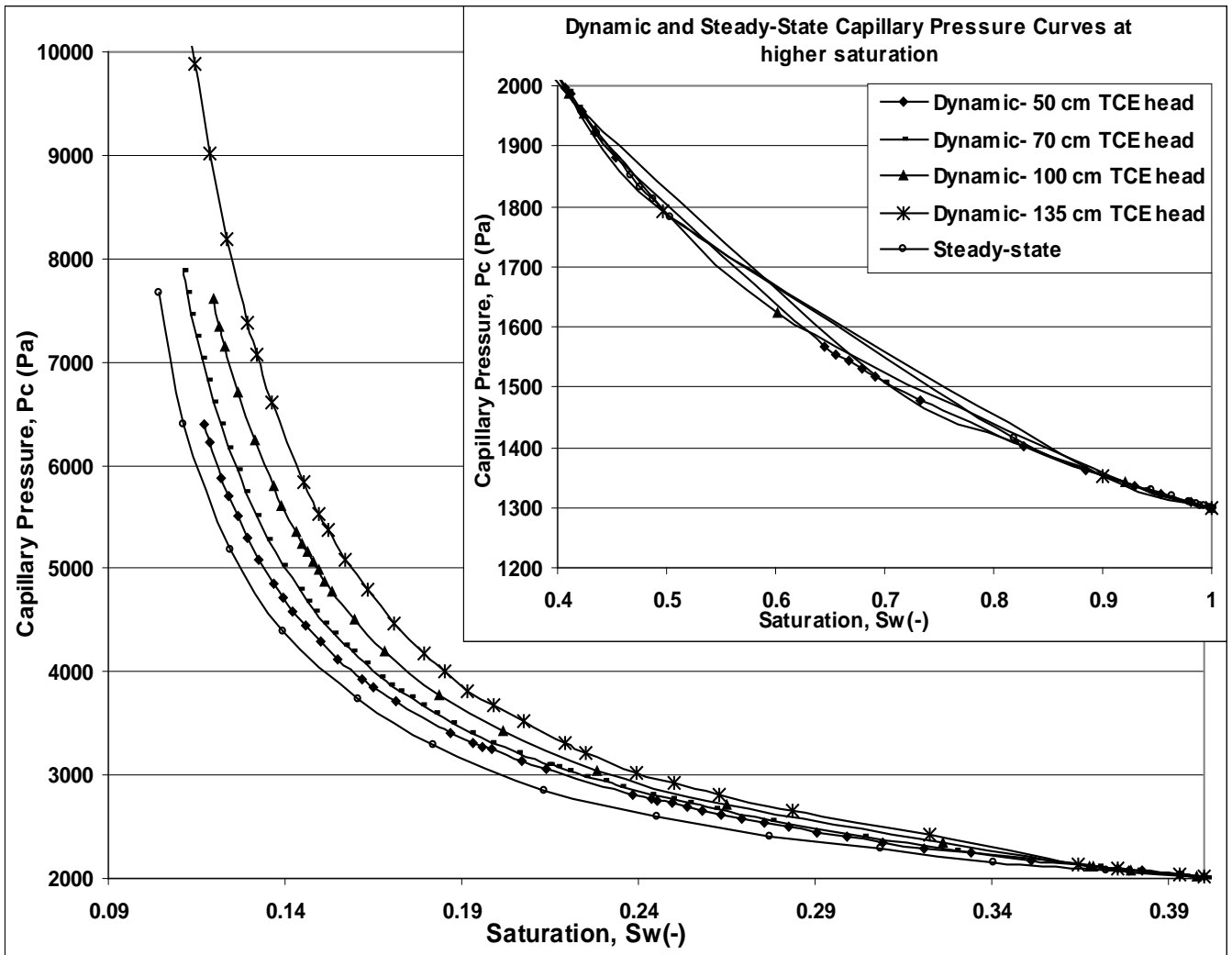


Figure 2. Steady-state and Dynamic Capillary Pressure-Saturation Curves for 3D Fine Sand Domain (homogeneous). The box shows the curves at higher water saturation.

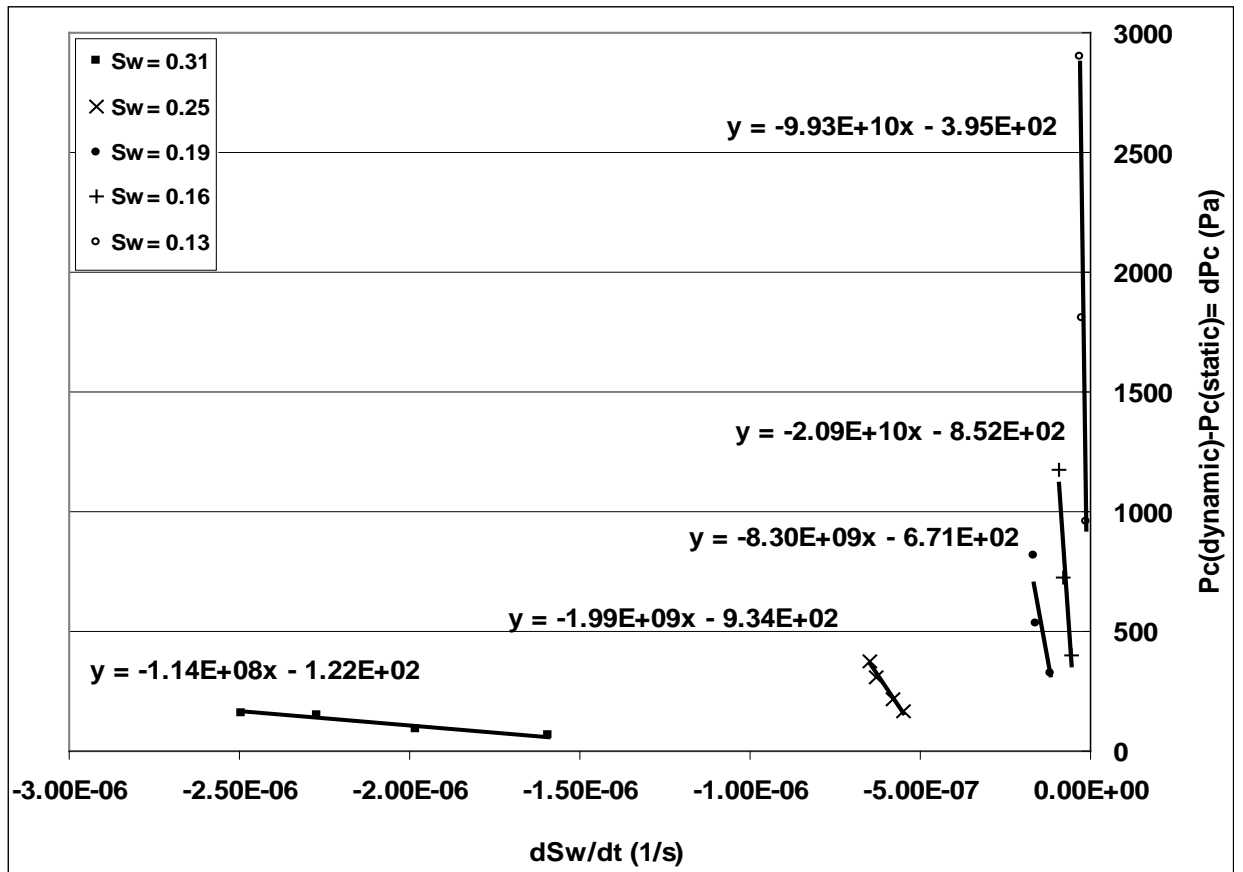


Figure 3(a)

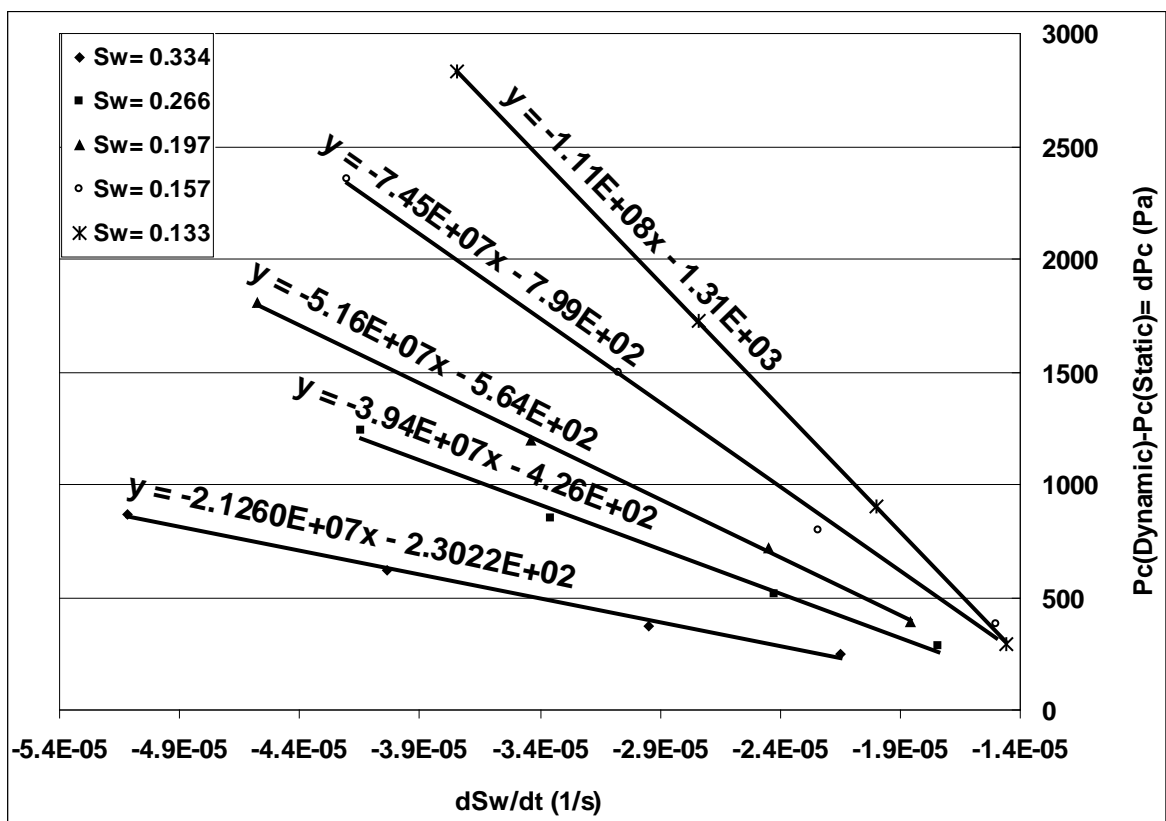


Figure 3(b)

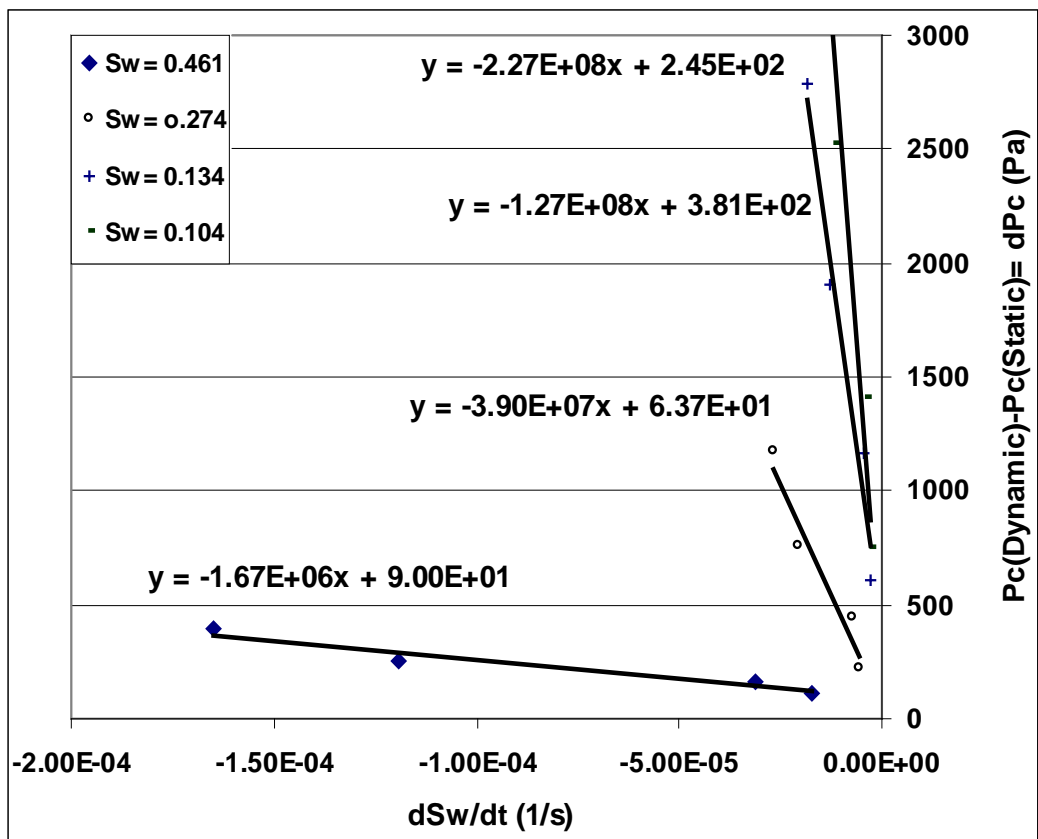


Figure 3(c)

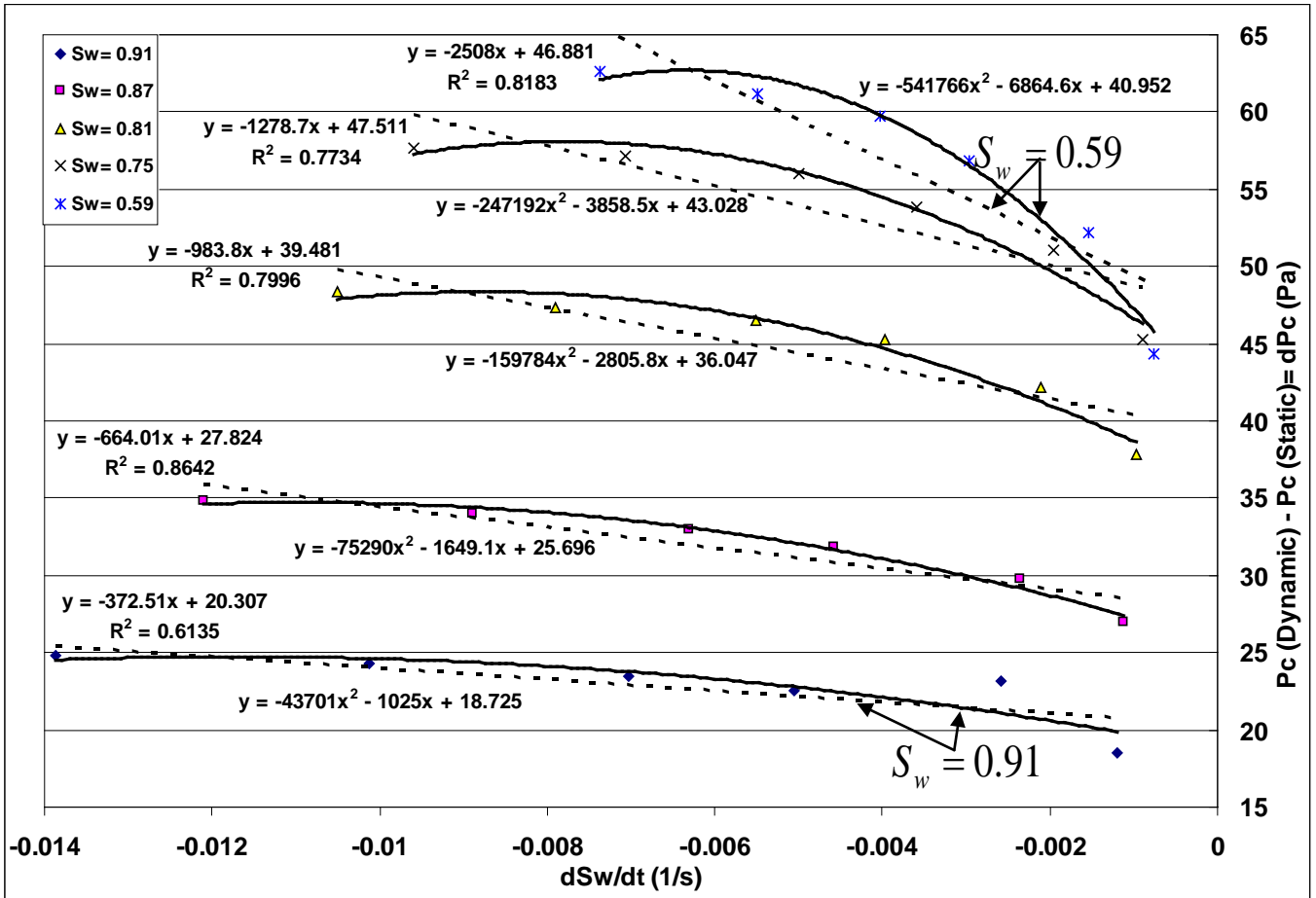


Figure 3(d)

Figure 3(a-d). Dynamic coefficient for (a) fine sand, (b) coarse sand, (c) heterogeneous sample with intensity of heterogeneity (ω) of 0.207 and, (d) fine sand at high saturations values. All simulations are carried out for 3D cylindrical samples (see, Figures 1 and 5).

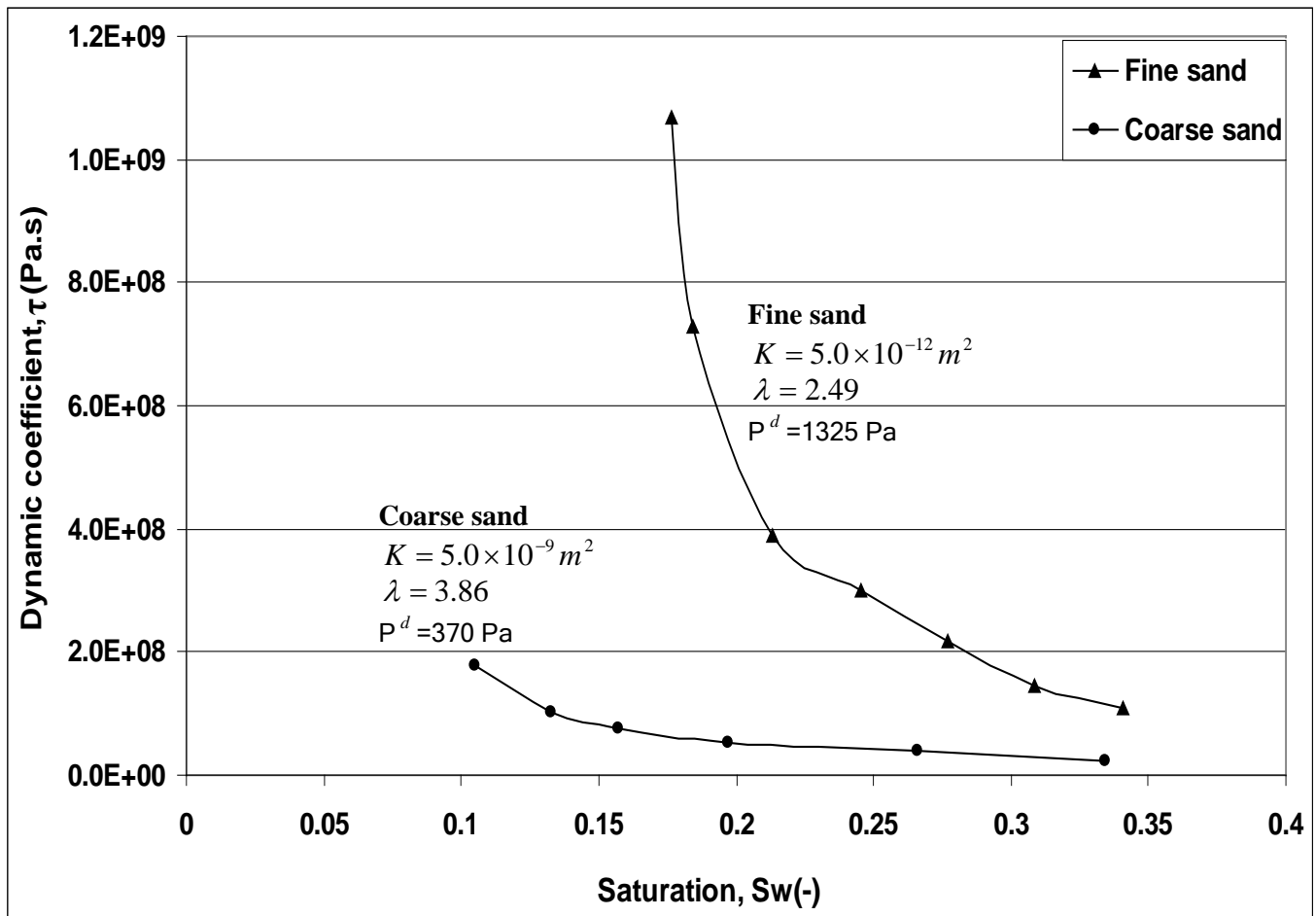


Figure 4. Pore size distribution (λ) and permeability (K) effects on dynamic coefficient (τ) value as a function of average saturation in a homogeneous cylindrical column consisting of either fine or coarse sand.

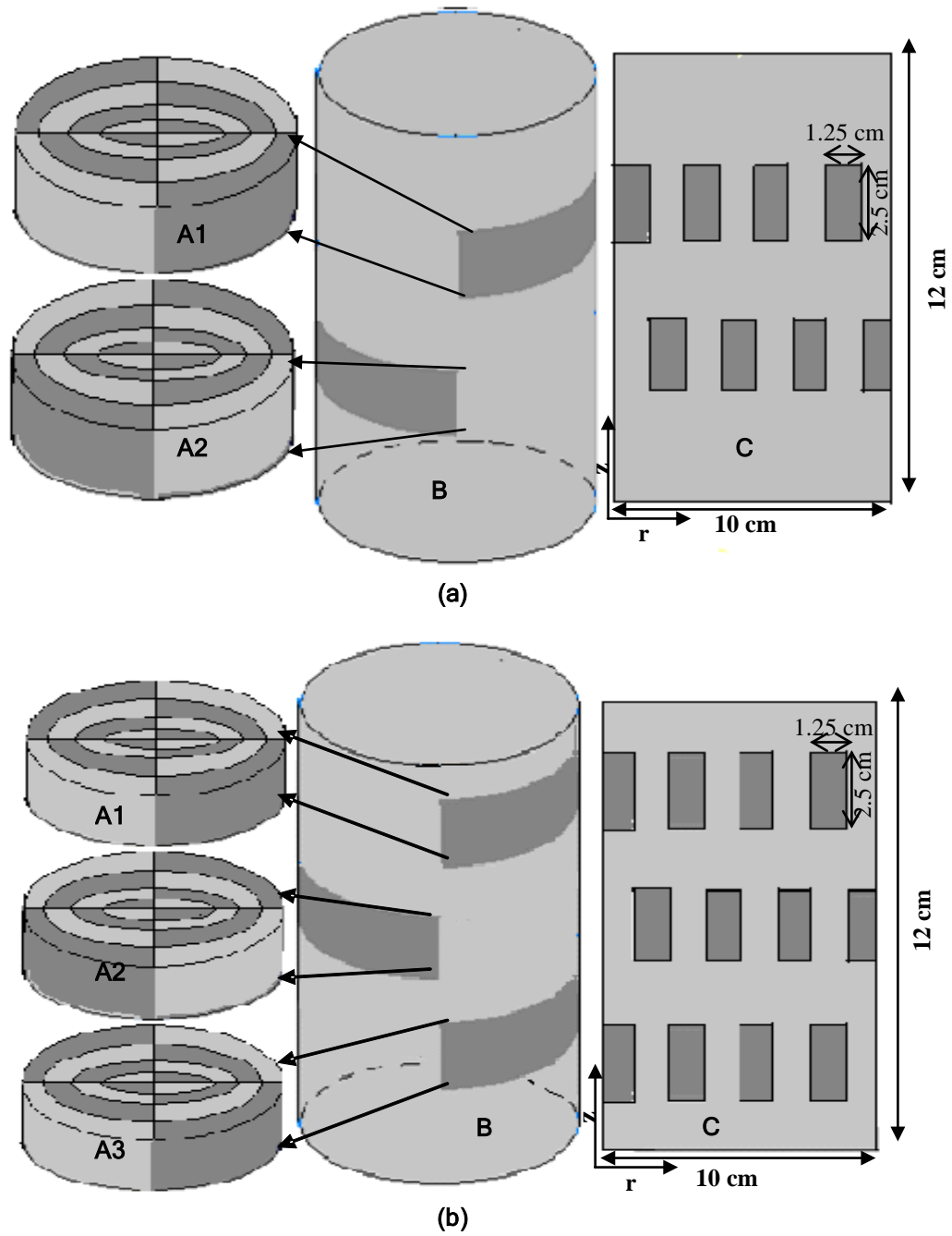


Figure 5 (a-b). 3D cylindrical domains for two intensities (ω) and distributions of micro-heterogeneities in the form of sub-sample scale fine sand blocks (dark grey regions) embedded in coarse sand background: (a) $\omega=0.207$ and (b) $\omega=0.372$.

(A1, A2, and A3) r - θ sections of heterogeneity distribution

(B) 3D heterogeneous sample displayed in cylindrical domain

(C) 2D rectangular (r - Z) section of heterogeneity distribution in cylindrical domain

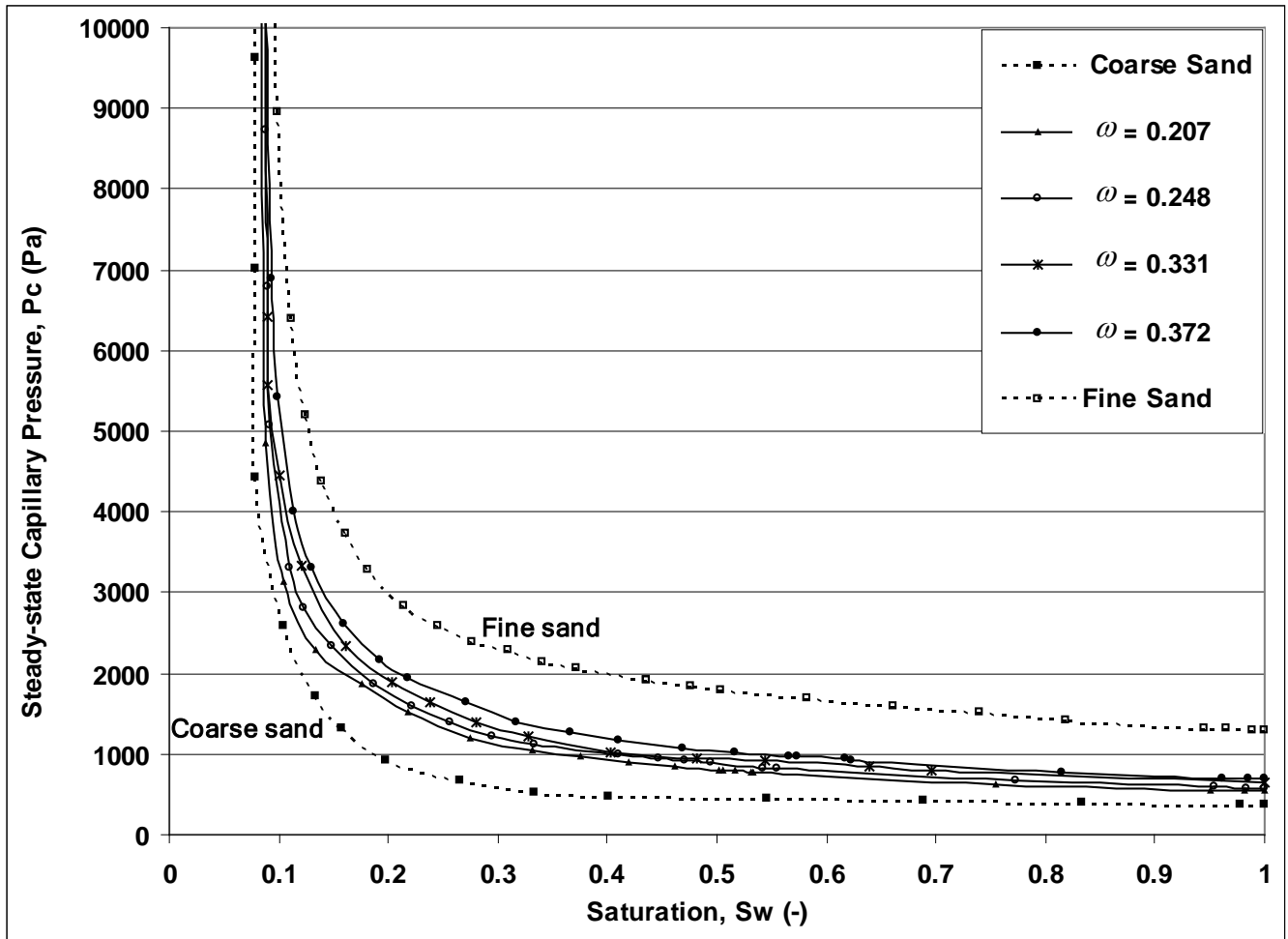


Figure 6(a)

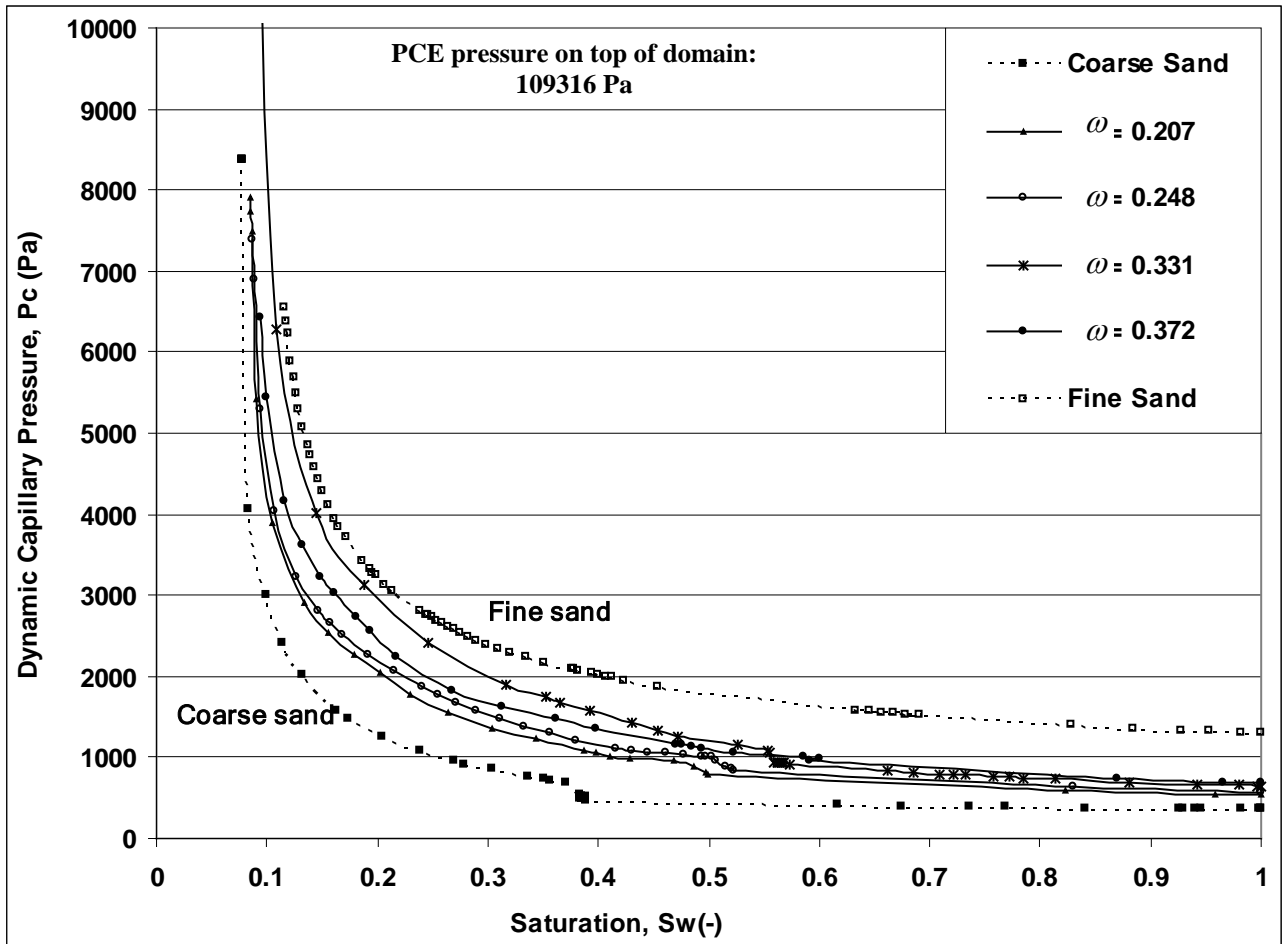


Figure 6(b)

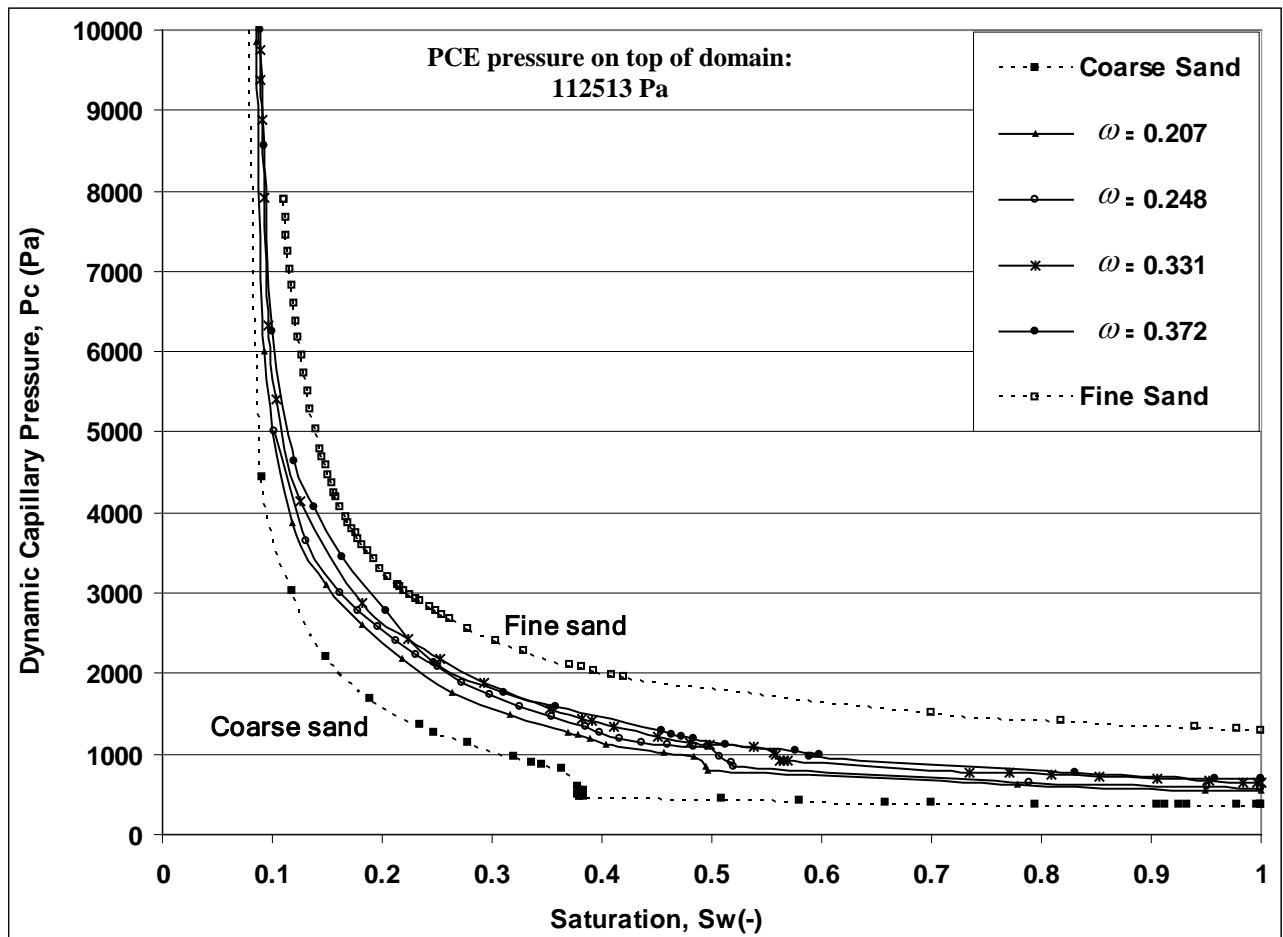


Figure 6(c)

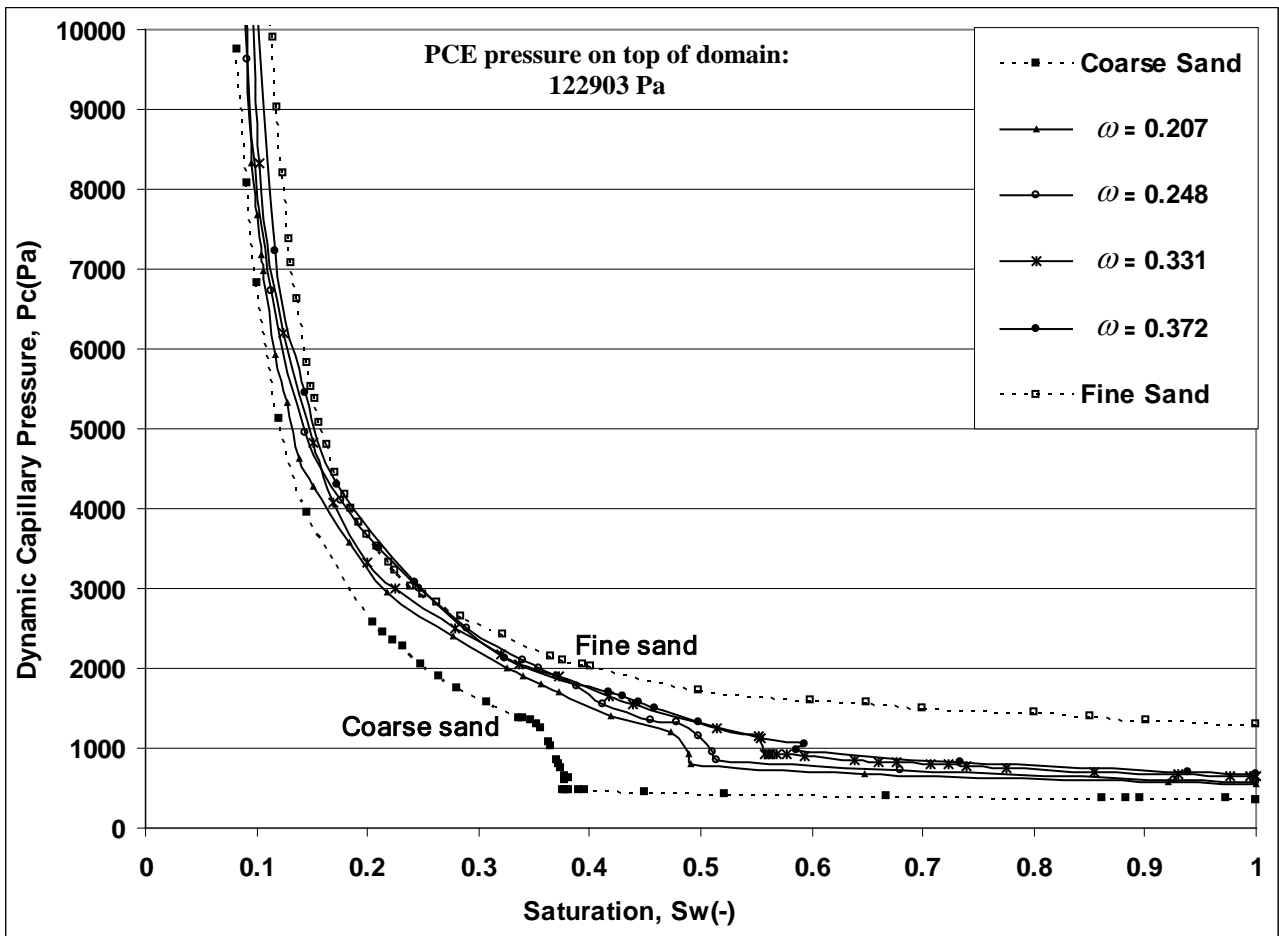


Figure 6(d)

Figure 6(a-d). Micro-Heterogeneity effects on (a) Steady-State and, Dynamic P^c - S curves for PCE pressure of (b) 109316 Pa, (c) 112513 Pa, and (d) 122903 Pa applied at the top of a cylindrical domain with various intensities of heterogeneity (ω). All results are for downward flow of PCE in cylindrical domains (3D).

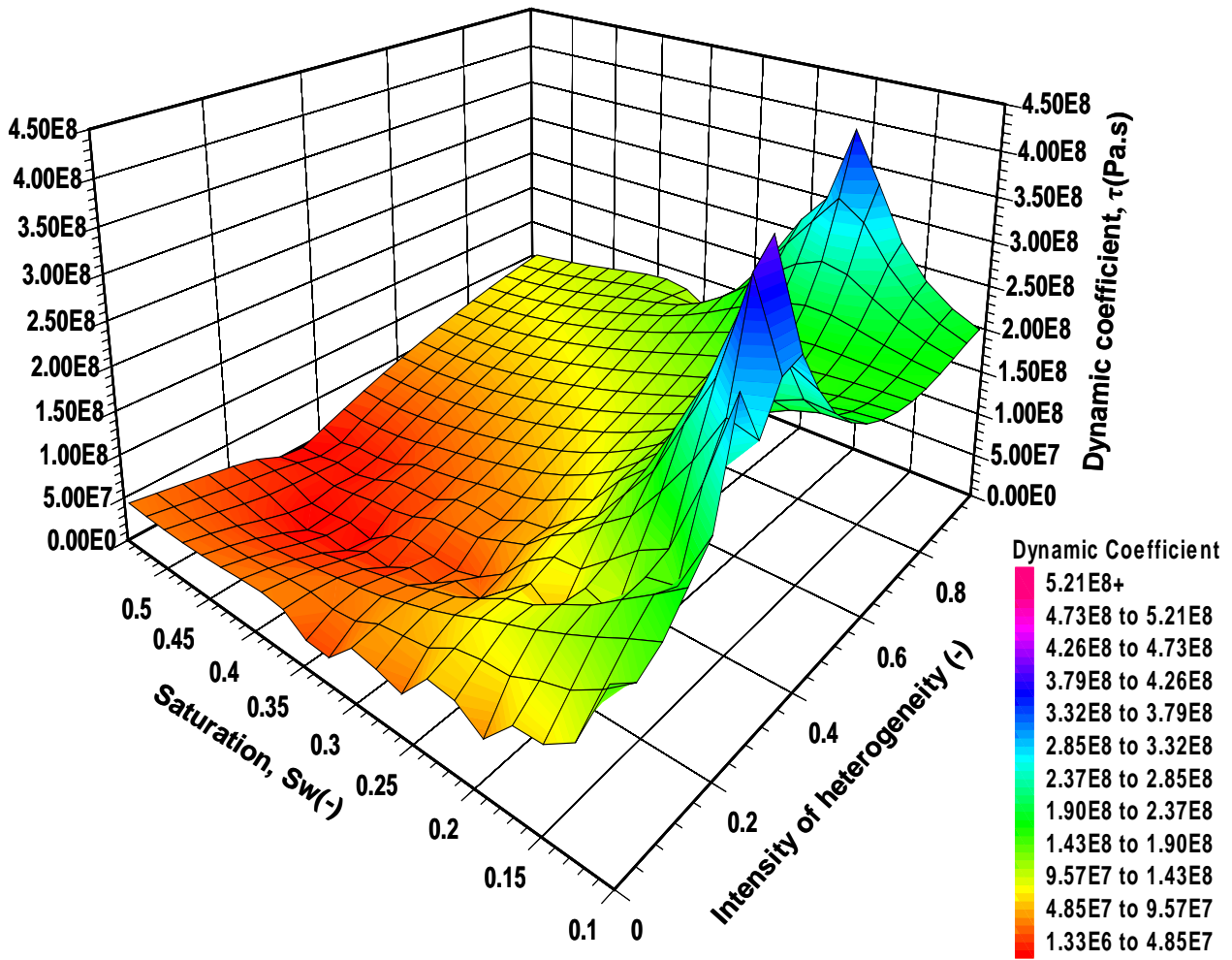


Figure 7. The effect of intensity of heterogeneity (ω) on dynamic coefficient (τ). The value of τ is calculated for a 3D cylindrical domain (ID= 10 cm and height =12 cm) composed of either fine sand ($\omega = 1$) or coarse sand ($\omega = 0$) for homogeneous domains and fine sand lenses imbedded in coarse sand for heterogeneous domains.

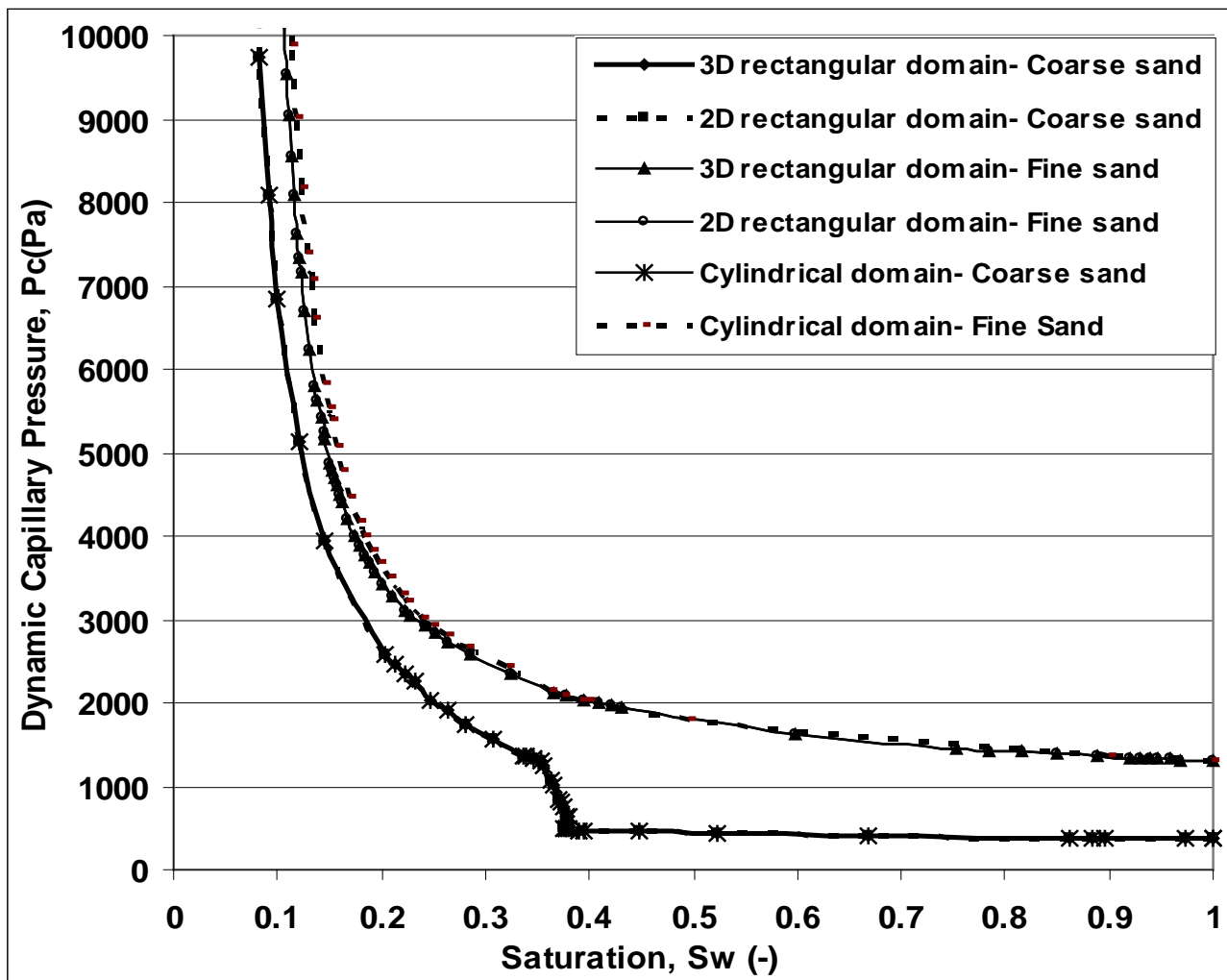


Figure 8(a)

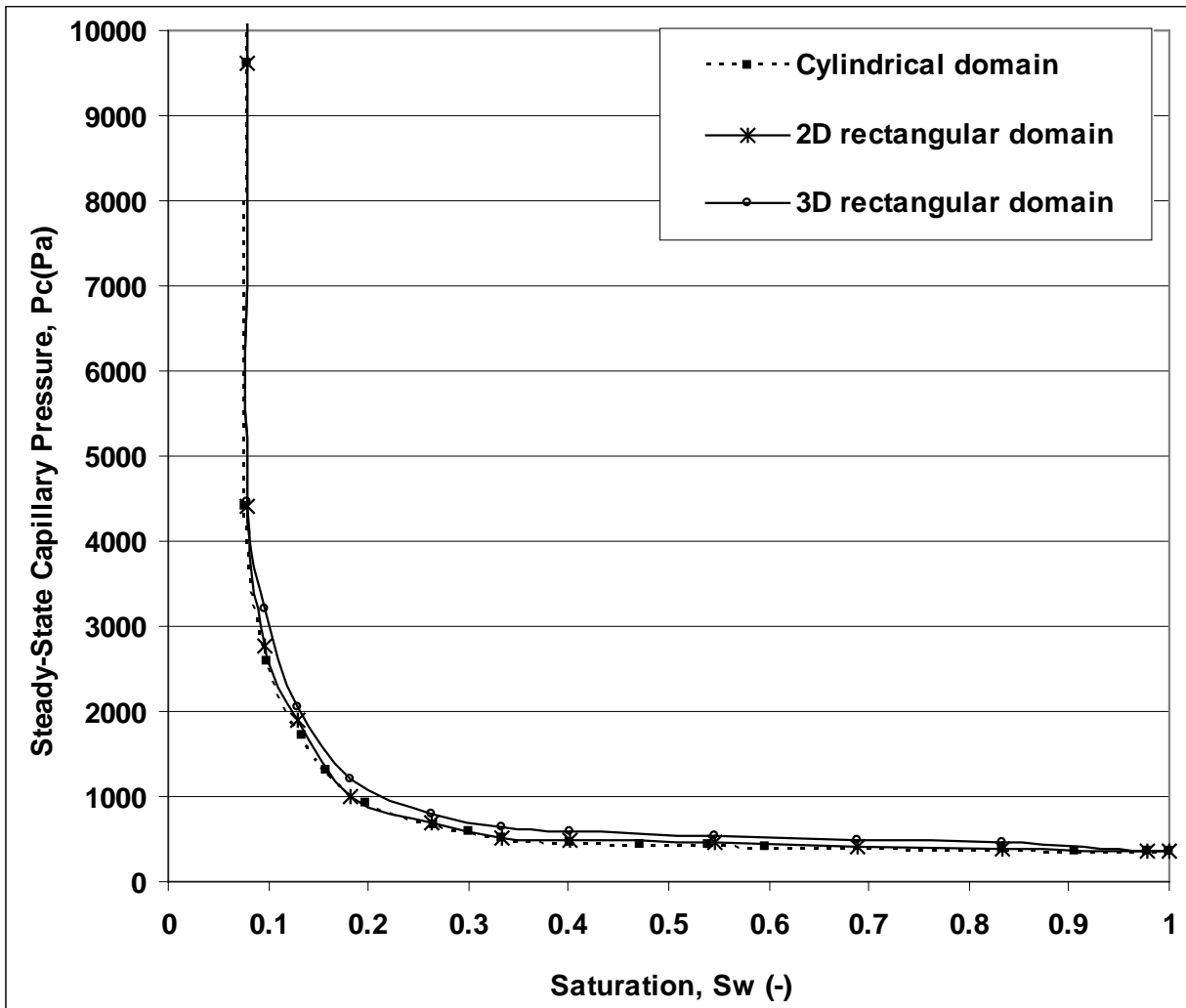


Figure 8(b)

Figure 8. (a) Effective dynamic capillary pressure curves for coarse and fine sand domain (b) Effective steady-state capillary pressure curves for coarse sand in different domain geometries. For fine sand the same trends are observed.

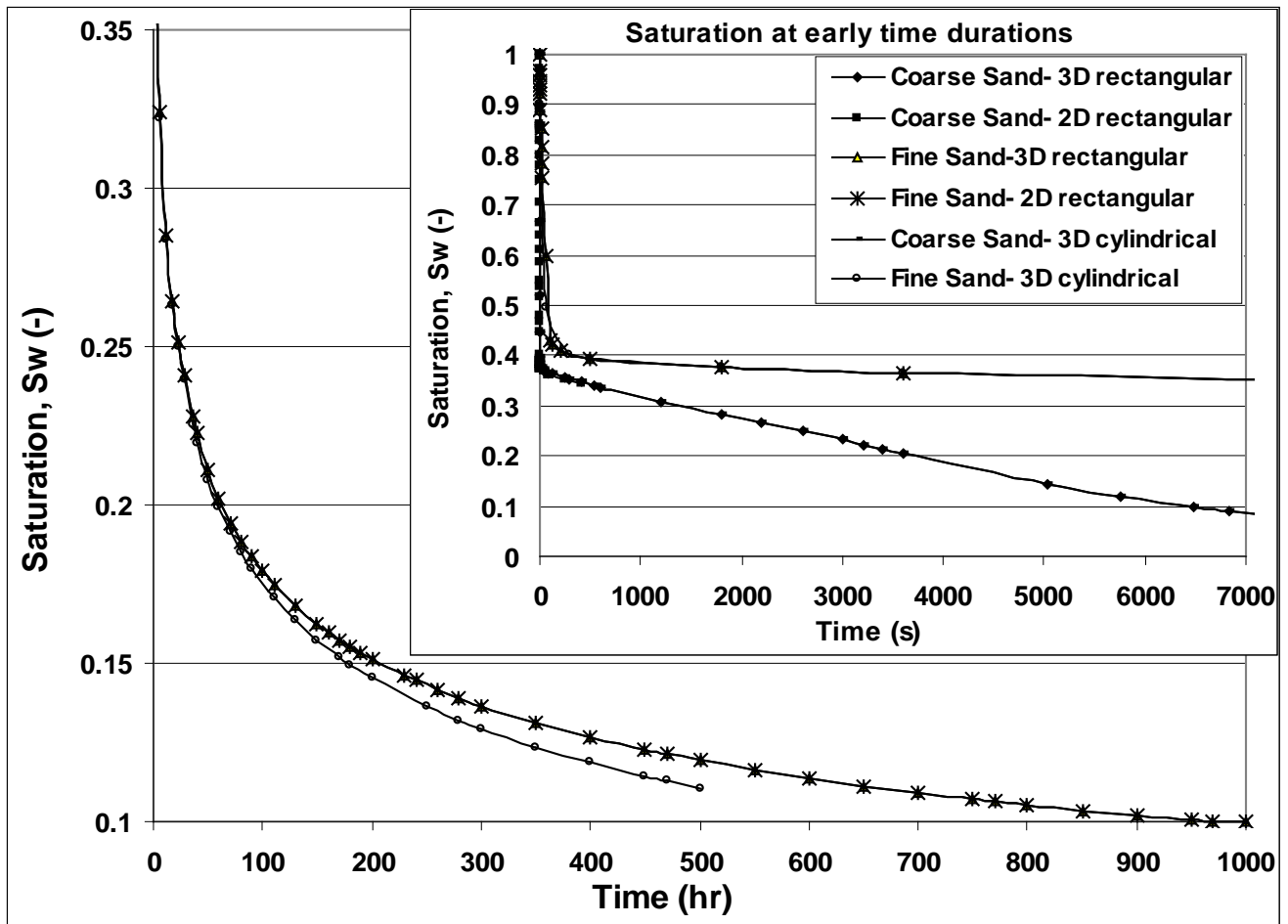


Figure 9. Saturation profile for coarse sand (in the box) and fine sand considering different domain geometries under dynamic flow condition. Saturation decrease rapidly in coarse sand sample (in less than 2 hours) because of high velocity fluid flow in large pore spaces and fast displacement of water by PCE in vertically downward flow.

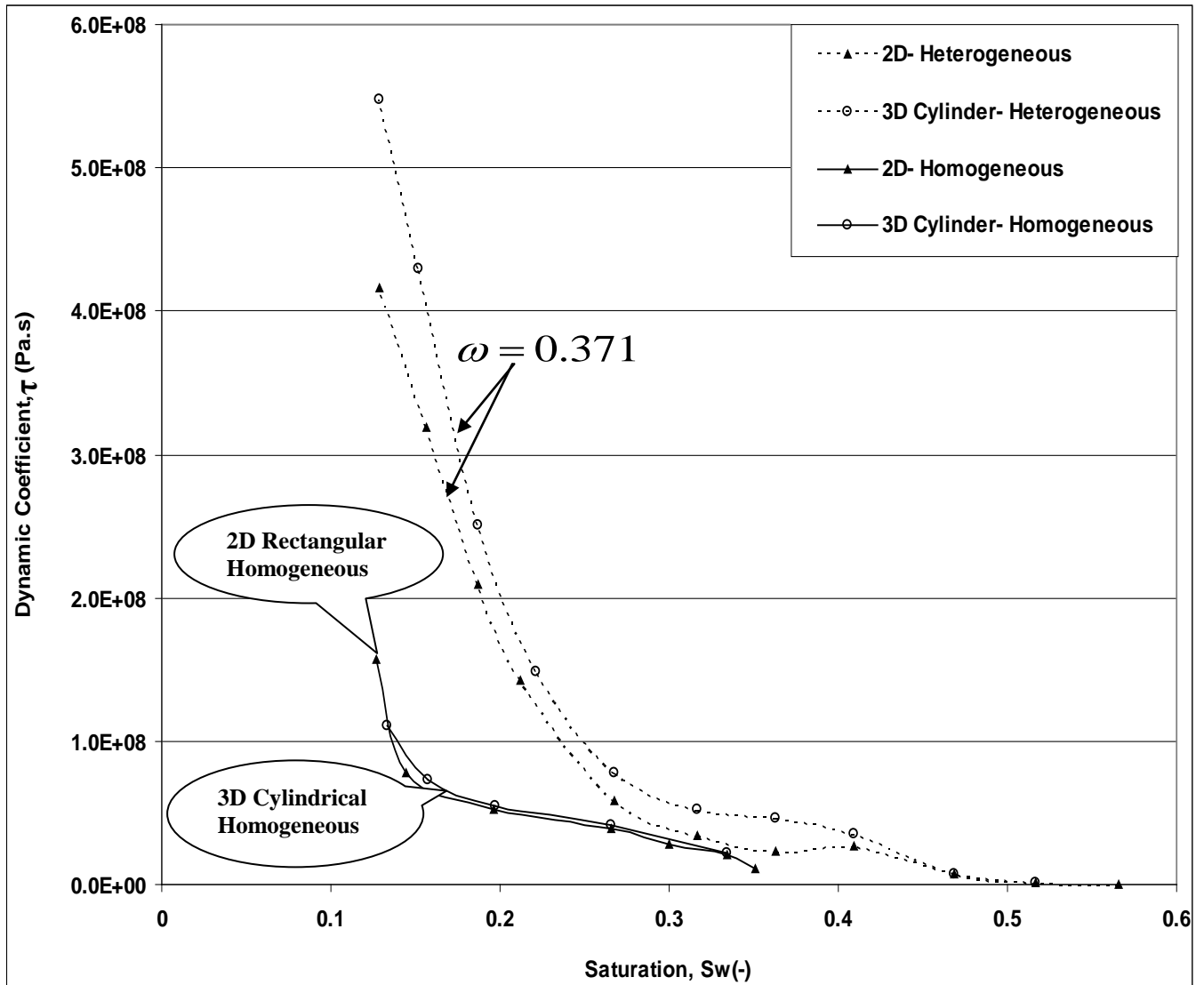


Figure 10. Domain geometry effects on dynamic coefficient. Geometry slightly affects the dynamic coefficient (τ) for flow in homogeneous coarse sand and heterogeneous domains for the geometry and dimensions shown in Figure 1.

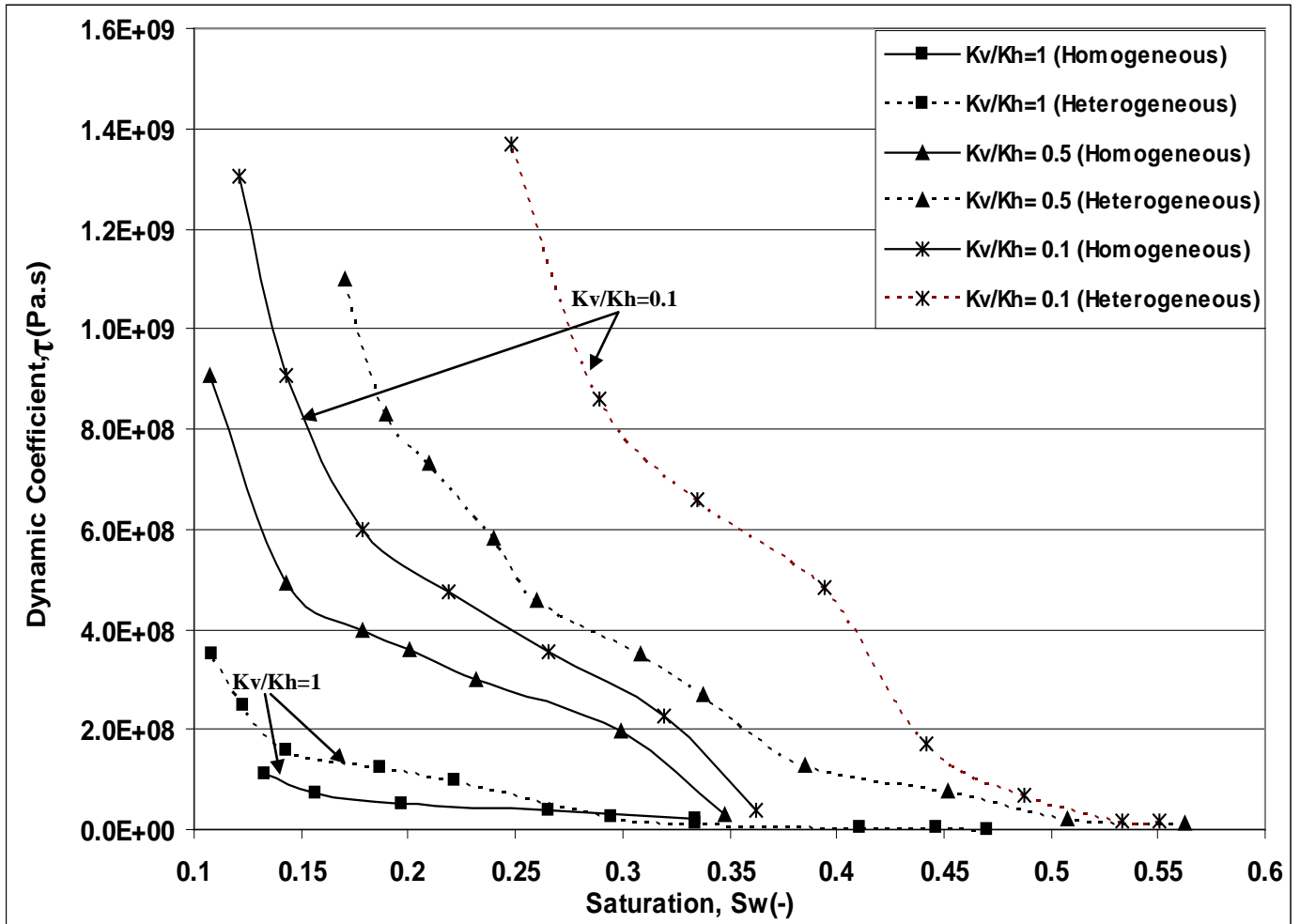


Figure 11. Effects of permeability anisotropy on dynamic coefficient for homogeneous (solid lines) and heterogeneous (dashed lines) domain with intensity of heterogeneity (ω) = 0.207 . Anisotropy has been defines as the ratio of vertical permeability ($K_v = 5.0 \times 10^{-9}$) to the horizontal permeability (K_v / K_h) where horizontal permeability remains the same in all directions (angles).

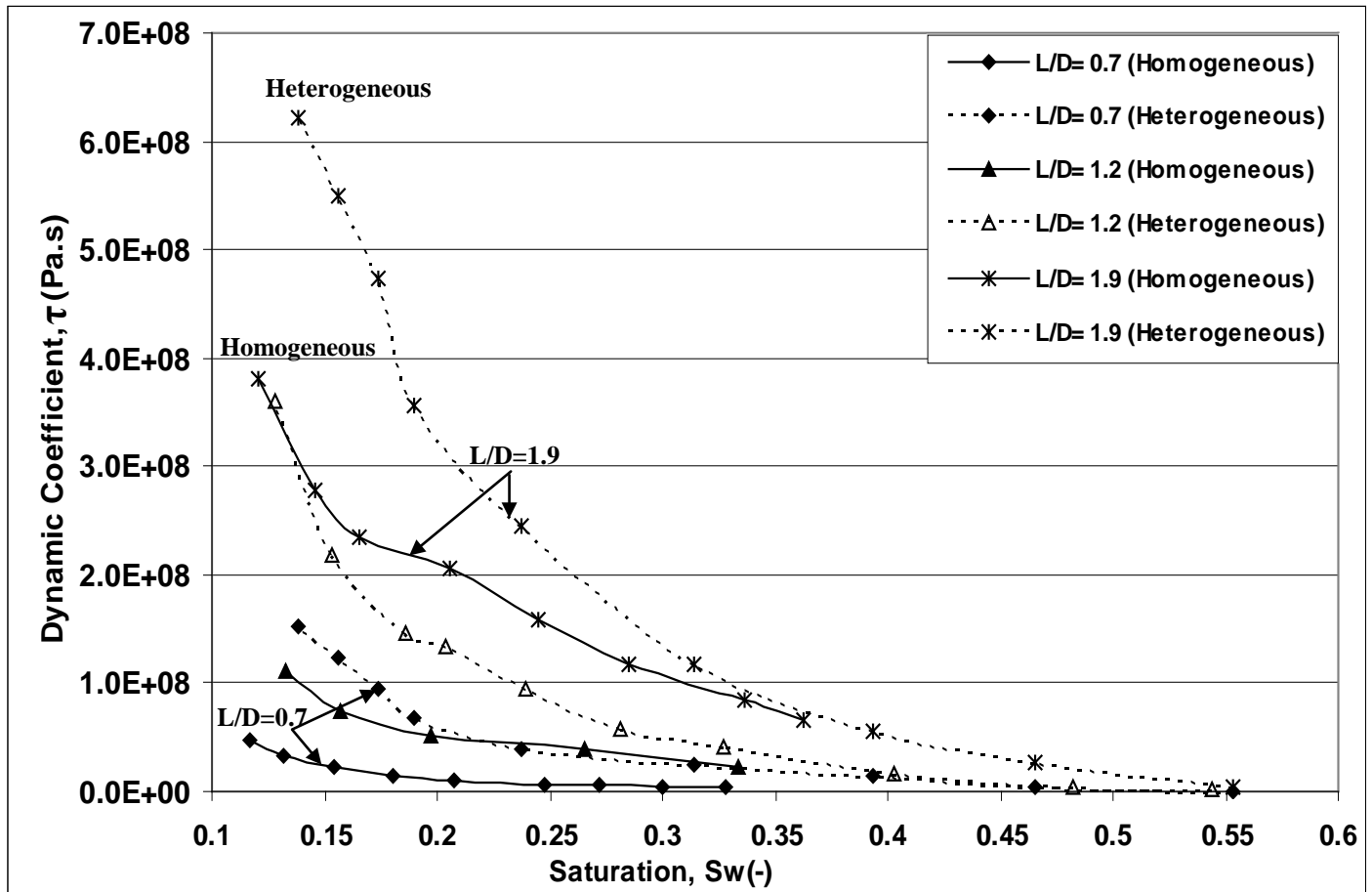


Figure 12. Effect of aspect ratio on dynamic coefficient for homogeneous and heterogeneous domains with intensity of heterogeneity (ω) = 0.331. Aspect ratio for cylindrical domain has been defined as Length/Diameter (L/D). In all cases the diameter (D) is kept constant while the length (L) is varied to obtain various L/D ratios.